Global model comparison of heterogeneous ice nucleation parameterizations in mixed phase clouds

Yuxing Yun[1] and Joyce E. Penner[1]

Received 6 July 2011; revised 27 January 2012; accepted 3 February 2012; published 4 April 2012.

[1] A new aerosol-dependent mixed phase cloud parameterization for deposition/condensation/immersion (DCI) ice nucleation and one for contact freezing are compared to the original formulations in a coupled general circulation model and aerosol transport model. The present-day cloud liquid and ice water fields and cloud radiative forcing are analyzed and compared to observations. The new DCI freezing parameterization changes the spatial distribution of the cloud water field. Significant changes are found in the cloud ice water fraction and in the middle cloud fractions. The new DCI freezing parameterization predicts less ice water path (IWP) than the original formulation, especially in the Southern Hemisphere. The smaller IWP leads to a less efficient Bergeron-Findeisen process resulting in a larger liquid water path, shortwave cloud forcing, and longwave cloud forcing. It is found that contact freezing parameterizations have a greater impact on the cloud water field and radiative forcing than the two DCI freezing parameterizations that we compared. The net solar flux at top of atmosphere and net longwave flux at the top of the atmosphere change by up to 8.73 and 3.52 W m^{-2}, respectively, due to the use of different DCI and contact freezing parameterizations in mixed phase clouds. The total climate forcing from anthropogenic black carbon/organic matter in mixed phase clouds is estimated to be 0.16–0.93 W m^{-2} using the aerosol-dependent parameterizations. A sensitivity test with contact ice nuclei concentration in the original parameterization fit to that recommended by Young (1974) gives results that are closer to the new contact freezing parameterization.

Citation: Yun, Y., and J. E. Penner (2012), Global model comparison of heterogeneous ice nucleation parameterizations in mixed phase clouds, *J. Geophys. Res.*, *117*, D07203, doi:10.1029/2011JD016506.

1. Introduction

[2] Mixed phase clouds (clouds that typically occur between 0°C and −40°C and contain both ice particles and supercooled liquid droplets) cover about 22% of the Earth [*Warren et al.*, 1986, 1988] and have a substantial influence on climate. The radiative properties of mixed phase clouds are largely determined by their cloud liquid water content, ice water content, as well as the number concentrations in each condensate type [*Xie et al.*, 2008]. Liquid droplets tend to be smaller and much more numerous than ice crystals, so the optical depth of a liquid cloud will be larger than an ice cloud with the same amount of condensed water. *Penner et al.* [2001] showed that the difference in forcing associated with changing all clouds between 0°C and −40°C from liquid to ice was +13 W m^{-2}. This forcing estimate included the effect of precipitation rate changes through their impacts on the ice and liquid water path (LWP) changes [*Lohmann*, 2002].

[3] At the warm temperatures in mixed phase clouds, ice particles are formed by various heterogeneous freezing processes, since homogeneous freezing requires high ice supersaturations, and is usually limited to temperatures below −40°C [*Pruppacher and Klett*, 1997]. During heterogeneous freezing (as opposed to homogeneous freezing), a so-called ice nucleus (IN) facilitates the phase transition from vapor or liquid to ice [*Pruppacher and Klett*, 1997]. Heterogeneous freezing occurs by four different mechanisms: condensation freezing, immersion freezing, deposition nucleation, and contact freezing. Condensation freezing occurs when a nucleus acts first as a cloud condensation nucleus and later as a freezing nucleus. Immersion freezing occurs when ice nucleates on a solid particle, which is immersed in a droplet. Deposition nucleation refers to the process by which water vapor directly deposits on a solid surface and freezes. Contact freezing refers to the freezing of a supercooled droplet when it collides with a freezing nucleus by Brownian diffusion, thermophoresis, or diffusiophoresis. These heterogeneous freezing mechanisms are described in more detail by *Vali* [1985].

[4] Variations in the number concentration and chemical properties of ice-forming nuclei in space and time should be taken into account when predicting ice number concentrations

[1]Department of Atmospheric, Oceanic, and Space Sciences, University of Michigan, Ann Arbor, Michigan, USA.

0148-0227/12/2011JD016506

in mixed phase clouds. However, the ice nucleation parameterization in mixed phase clouds in most GCMs does not depend on the aerosol properties. For example, the *Cooper* [1986] and *Fletcher* [1962] parameterizations are only a function of temperature. The *Meyers et al.* [1992] parameterization that is often used for deposition and condensation freezing only depends on supersaturation. Also, the *Meyers et al.* [1992] parameterization was derived from measurements near the surface and thus will overpredict the ice crystal concentrations, if adjustments are not made to account for the decrease in aerosol particles with altitude. Due to these limitations one cannot use these ice nucleation parameterizations to study the effects of aerosols on mixed phase clouds.

[5] Recently, several heterogeneous freezing parameterizations have been developed to take into account the effects of different aerosol types on ice nucleation. Some of these are based on laboratory observations [*Lohmann and Diehl*, 2006; *Diehl and Wurzler*, 2004; *Diehl et al.*, 2006; *Marcolli et al.*, 2007; *Connolly et al.*, 2009; *Murray et al.*, 2011]. Some of the laboratory observations used artificially generated surrogates for atmospheric particles [*DeMott*, 1990; *Diehl and Mitra*, 1998; *Gorbunov et al.*, 2001; *Murray et al.*, 2011], while others used natural aerosol samples [*Schaefer*, 1949; *Isono and Ibeke*, 1960; *Field et al.*, 2006; *Connolly et al.*, 2009; *Koehler et al.*, 2007, 2010; *Kulkarni and Dobbie*, 2010; *Kanji et al.*, 2011]. Another group of heterogeneous freezing parameterizations are based on classical nucleation theory. The problem with using classical nucleation theory is that the freezing ability of an aerosol particle is characterized by the contact angle parameter, which is hard to measure and validate. In addition, the use of a single contact angle for differentiating the freezing properties of different particle types also assumes that the substrate surface is energetically homogeneous. In reality, it is thought that freezing preferentially starts at certain active sites on certain particles [*Pruppacher and Klett*, 1997, p. 330]. Several studies have utilized the classical nucleation theory and made various improvements [*Kärcher and Lohmann*, 2003; *Chen et al.*, 2008; *Marcolli et al.*, 2007; *Khvorostyanov and Curry*, 2004; *Liu and Penner*, 2005; *Pruppacher and Klett*, 1997, pp. 341–344]. A third method for deriving heterogeneous freezing parameterizations is to develop an empirically derived in situ observation-based parameterization. This was the method used by *Phillips et al.* [2008], who proposed a parameterization for deposition/condensation/immersion (DCI) freezing that was constrained by in situ measurements of IN number concentration. In this parameterization, the number concentration of ice nuclei not only depends on ice supersaturation, but also on the surface area concentration, and the proportion of dust, black carbon, and organics. *Eidhammer et al.* [2009] compared three heterogeneous ice nucleation parameterizations in a parcel model including the in situ observation-based method of *Phillips et al.* [2008], the *Khvorostyanov and Curry* [2004] parameterization which is based on classical theory, and the *Diehl and Wurzler* [2004] parameterization which is based on laboratory observations, and they concluded that the *Phillips et al.* [2008] parameterization compares well with most ice nucleation measurements included in their study. They recommended that it be used in cloud and global-scale models in preference to the other two parameterizations. Recent implementations of the *Phillips et al.* [2008] parameterization include *Seifert et al.* [2011], who implemented the *Phillips et al.* [2008] parameterization in a convective-scale weather prediction model; *Wang et al.* [2011], who implemented it in a regional climate model; and *Barahona et al.* [2010], who implemented it for cirrus clouds in a global model. *DeMott et al.* [2010] proposed a simplified version of the *Phillips et al.* [2008] parameterization, which depends on the total nonsea-salt aerosol number concentration with diameter larger than 0.5 μm instead of relying on the surface area of dust, black carbon, and organics separately. However, here we choose to implement the *Phillips et al.* [2008] parameterization since it specifically includes the separate effects of organics, BC, and dust particles.

[6] For contact freezing, there is no parameterization available that is constrained by in situ measurements. The commonly applied *Young* [1974] parameterization predicts contact ice nuclei number concentrations based on temperature and was derived from the experimental data of *Blanchard* [1957]. It does not consider the specific properties of the aerosols that may affect contact freezing. In this parameterization, the number concentration of contact ice nuclei below -4°C is calculated as a temperature scaling of a specified number concentration of active ice nuclei at -4°C. *Phillips et al.* [2008] proposed a contact freezing parameterization based on the assumption that each IN particle can nucleate ice at a freezing temperature that is 4.5°C higher than the freezing temperature associated with immersion or condensation freezing. This assumption was based on laboratory observations reported by *Shaw et al.* [2005]. Using this method, one is able to use the aerosol-dependent Phillips deposition/condensation/immersion freezing parameterization to treat contact freezing by specific aerosol types. However, the drawback of not being constrained by in situ observations still exists.

[7] Several recent studies have focused on heterogeneous ice nucleation in mixed phase clouds using General Circulation Models (GCM). *Salzmann et al.* [2010] and *Gettelman et al.* [2010] improved the microphysics scheme in GFDL AM3 and CAM, respectively, and found that the simulated cloud forcing is sensitive to the formulation of the ice microphysics. *Hoose et al.* [2010] implemented a classical-theory-based heterogeneous freezing parameterization in CAM-Oslo, and found that immersion freezing by dust is the dominant ice formation process, while the contribution of biological aerosols is marginal. *Lohmann et al.* [2007], *Lohmann and Hoose* [2009], and *Storelvmo et al.* [2008, 2011] investigated the aerosol indirect effect in general, or in mixed phase clouds only, and found that mixed phase cloud process have a major effect on the anthropogenic aerosol effect. In this study, we extend the previous studies by implementing the two *Phillips et al.* [2008] parameterizations in the coupled CAM and IMPACT aerosol transport model [*Wang and Penner*, 2010; *Wang et al.*, 2009], and compare these formulations to the previously used *Meyers et al.* [1992] parameterization and *Young* [1974] parameterization. This new set of heterogeneous freezing parameterizations has empirically derived dependencies on the chemistry and surface area of multiple aerosol species. This allows us to examine the climate forcing of anthropogenic aerosols on mixed phase clouds. A total of 6 model

simulations are presented. Ice nuclei number concentration, cloud liquid water path, ice water path, and the Earth's radiation budget from the different simulations are compared among themselves and to satellite observations. We also present an estimate of the anthropogenic aerosol effect in mixed phase clouds in the two simulations with the aerosol-dependent deposition/condensation/immersion freezing parameterization and each of the two contact freezing parameterizations. In section 2, we describe the coupled model setup in detail, as well as the four heterogeneous freezing parameterizations we test. Sections 3.1–3.7 discuss results for the ice nuclei concentrations, the cloud liquid/ice fields, the top of the atmosphere (TOA) radiation fields, as well as the comparison to satellite observations. We present the effects of anthropogenic black carbon/organic matter (BC/OM) on mixed phase clouds in section 3.8. A sensitivity test that examines the effect of tuning the reference contact IN to that assumed in the *Young* [1974] parameterization is discussed in section 3.9. Section 4 concludes the study and provides an outlook for future developments.

2. Methods

2.1. The CAM-IMPACT Model

[8] In this study, we use the coupled CAM-IMPACT model. The coupled model consists of two components: the NCAR Community Atmospheric Model (CAM3) [*Collins et al.*, 2006a], and the University of Michigan (Umich) IMPACT aerosol model (which is derived from the Lawrence Livermore National Laboratory (LLNL) chemical transport model) [*Rotman et al.*, 2004; *Penner et al.*, 1998]. The two components are run concurrently in the multiple processors multiple data (MPMD) mode [*Wang et al.*, 2009].

2.1.1. The IMPACT Global Aerosol Model

[9] Umich IMPACT aerosol model is developed to use massively parallel computer architectures. *Liu and Penner* [2002] modified the LLNL IMPACT atmospheric chemistry model to treat the mass of sulfate aerosol as a prognostic variable. The model was further extended by *Liu et al.* [2005] to simulate the microphysics of sulfate aerosol and its interactions with primary nonsulfate aerosols based on the aerosol module developed by *Herzog et al.* [2004]. The primary nonsulfate aerosol components included in this study are natural organic matter (NOM), which is assumed to be formed from terpene emissions, fossil fuel burning black carbon and organic matter (FFBC/OM), biomass burning black carbon and organic matter (BBBC/OM), aircraft BC (ABC), dust, and sea salt. Dust, sea salt, black carbon/organic matter are internally mixed with sulfate. The internal mixtures are formed through coagulation with sulfate aerosols, condensation of sulfuric acid, and when sulfate is formed through aqueous reactions in cloud drops that contain nonsulfate aerosols. Although BC and OM from fossil fuel burning and biomass burning are treated as distinct species in the model, they are assumed to be internally mixed for both optical properties and their effects on ice [*Liu et al.*, 2005; *Wang and Penner*, 2010]. The *Herzog et al.* [2004] module is able to treat an arbitrary number of modes to describe the microphysical processes determining the distribution of sulfate aerosol and its mixing state with other aerosol types [*Herzog et al.*, 2004; *Liu et al.*, 2005]. Here we used the three-mode version that describes the variation of pure sulfate in a nucleation mode (radius < 5 nm), an Aitken mode (5 nm < radius < 50 nm), and an accumulation mode (radius > 50 nm). Both the mass and number of the pure sulfate aerosol for the three modes are predicted. Mineral dust and sea salt are divided into four size bins with radii varying from 0.05 to 0.63 μm, 0.63–1.26 μm, 1.26–2.5 μm, and 2.5–10 μm. Carbonaceous aerosols (BC and OM) are represented by a single submicron size bin. For a complete list of the size distribution parameters for nonsulfate aerosols, see *Liu et al.* [2005, Table 3]. The other predicted species include: dimethylsulfide (DMS), sulfur dioxide (SO_2), and hydrogen peroxide (H_2O_2). A detailed description of the formation of sulfate particles, their interaction with nonsulfate aerosols, dry deposition, wet deposition and the scavenging efficiencies, as well as comparisons with observations is given by *Wang et al.* [2009]. The present aerosol module uses the sea salt emissions calculated online in the model based on the work by *Monahan and O'Muircheartaigh* [1986], and anthropogenic emissions set to those for the year 2000 [*Penner et al.*, 2009]. In addition, natural emissions of dust, DMS from the oceans, OM from vegetation, and SO_2 from volcanoes are included. SO_2 and BC/OM from fossil fuel burning adjusted to represent the spatial distribution from land, ship, and aircraft transportation from QUANTIFY (http://www.pa.op.dlr.de/quantify) are included.

[10] The IMPACT aerosol model can be driven by either the meteorological fields from a general circulation model or assimilated meteorological data. In this coupled model study, we drive the IMPACT model by the generated meteorological fields from NCAR CAM3 as updated by *Wang and Penner* [2010]. Thus, variables such as temperature, wind speed, humidity, cloud water, cloud fraction, pressure, convective mass flux, precipitation, boundary layer height and detrainment rate are passed from CAM3 to IMPACT at each IMPACT advection time step.

2.1.2. NCAR CAM3

[11] The NCAR CAM3 is part of the Community Climate System Model 3 (CCSM3) [*Collins et al.*, 2006a, 2006b]. The model predicts both cloud liquid water and cloud ice water [*Boville et al.*, 2006]. The standard CAM3 version was updated by *Liu et al.* [2007], by introducing a two-moment cloud microphysics scheme for ice clouds, in which cloud ice number concentrations as well as mass concentrations are predicted by a prognostic equation. The two-moment scheme treats ice nucleation, coagulation, evaporation, and melting. In addition, *Wang and Penner* [2010] added a prognostic cloud droplet number concentration equation for liquid clouds. The complete set of equations for the two-moment treatment of cloud microphysics for liquid, ice, and mixed phase clouds can be found in the supplementary material of *Wang and Penner* [2010]. The cloud droplet activation parameterization is that of *Abdul-Razzak and Ghan* [2000, 2002]. The liquid/ice partitioning in mixed phase clouds is accomplished by explicitly treating the liquid mass conversion to ice due to the depositional growth of cloud ice at the expense of liquid water (the Bergeron-Findeisen process) using the scheme of *Rotstayn et al.* [2000]. This replaces the simple temperature-dependent liquid/ice partitioning in the standard CAM3. The cloud condensation and evaporation (C-E) scheme of *Zhang et al.* [2003] which removes any supersaturation above that of

liquid water in the standard CAM3 is used only for liquid water in warm and mixed phase clouds. In mixed phase clouds, water saturation is assumed for simplicity. Under such conditions, it is hard to distinguish deposition nucleation, condensation freezing, and immersion freezing. So here we refer to deposition/condensation/immersion freezing in mixed phase clouds. However, in reality deposition nucleation cannot happen if aerosols take up layers of water when water saturation is approached. A statistical cirrus cloud scheme that accounts for mesoscale temperature and velocity perturbations is implemented as described by *Wang and Penner* [2010] to better represent both subgrid-scale supersaturation and cloud formation. The treatment of temperature fluctuations with altitude is based on the gravity wave parameterization from *Gary* [2006, 2008]. We follow the *Wang and Penner* [2010] estimates for IN in cirrus clouds, which treated homogeneous freezing of pure sulfate particles and assumed that 1% of dust, BC/OM, and aircraft soot are immersion freezing IN [*Wang and Penner*, 2010].

[12] In CAM3, aerosol optical properties are calculated using a prescribed aerosol concentration from an off-line calculation constrained by an assimilation of satellite retrievals [*Collins et al.*, 2001; *Rasch et al.*, 2001]. In the coupled CAM-IMPACT model, the prescribed aerosol concentration from CAM3 is replaced with concentrations calculated in the IMPACT aerosol model.

2.2. Heterogeneous Ice Nucleation Parameterizations

2.2.1. Deposition/Condensation/Immersion Freezing

2.2.1.1. The Phillips DCI Freezing Parameterization

[13] *Phillips et al.* [2008] introduced a versatile method for parameterizing ice crystal number concentration in mixed phase as well as cirrus clouds. The fundamental assumption in this parameterization is that the number concentration of ice nuclei for each aerosol species is proportional to the surface area of its aerosol particle population. There is theoretical and observational evidence supporting this assumption [*Pruppacher and Klett*, 1997; *DeMott*, 1990]. Heterogeneous freezing is an interface phenomenon on the surface of the IN, initiated at specific "active sites." Given the same surface properties, the larger the IN particle, the more active sites it will have. *Georgii and Kleinjung* [1967], *Berezinski et al.* [1988], *Archuleta et al.* [2005] and *Santachiara et al.* [2010] examined the effect of size on ice nucleation and found that the nucleation efficiency at a given temperature and supersaturation increases with increasing particle size. The *Phillips et al.* [2008] parameterization is qualitatively consistent with these findings since the number of active IN of each aerosol species is assumed to be proportional to its total surface area. The ice nuclei number concentration resulting from each of the three species treated by *Phillips et al.* [2008] is calculated as

$$\mathrm{IN}_{DIC,X} = \int_{\log[0.1\mu\mathrm{m}]}^{\infty} \{1 - \exp[-\mu_{\mathrm{X}}(D_X, S_i, T)]\} \frac{dn_X}{d\log D_X} d\log D_X \tag{1}$$

where X is the label for the aerosol type (see Table 1 for definitions of variables used in this paper). In this study, X = Dust, or BC/OM (dust and black carbon/organic matter, respectively). S_i is the saturation ratio of vapor with respect to ice, and T is the physical temperature of ambient air in °C. BC/OM from both fossil fuel burning and biomass burning are included. A recent laboratory study [*Friedman et al.*, 2011] found out that bare and coated soot particles are poor deposition ice nuclei below water saturation. However, above water saturation, droplet and ice particles cannot be distinguished in their experiment. So the efficiency of deposition/condensation/immersion nucleation at water saturation cannot be inferred from their study. The mixed phase clouds in our model are assumed to be at water saturation. Therefore, BC/OM are considered as deposition/condensation/immersion nuclei in our study.

[14] The number mixing ratio of aerosols in group X is n_X; μ_X is the average of the number of activated ice embryos per insoluble aerosol particle in the size interval between D_X and $D_X + d\log D_X$ and is calculated as

$$\mu_X = H_X(S_i, T)\xi(T)\left(\frac{\alpha_X n_{\mathrm{IN},1,*}}{\Omega_{X,1,*}}\right)\frac{d\Omega_X}{dn_X} \tag{2}$$

where $n_{\mathrm{IN},1,*}$ is the number mixing ratio of ice nuclei for the reference conditions at water saturation. The reference condition for this parameterization is based on field observations made during the Ice Nuclei Spectroscopy (INSPECT) 1 campaign [*DeMott et al.*, 2003], which took place in North America and is thought to be representative of typical background free tropospheric conditions. However, the representativeness of this background free troposphere condition is limited by the available data. The parameter n_X is the number mixing ratio of particles in aerosol group X. Ω_X is the total surface area mixing ratio of all aerosols with dry diameters larger than 0.1 μm in group X, and $\Omega_{X,1,*}$ is the component of Ω_X in the background reference scenario. The values of $\Omega_{X,1,*}$ are taken from *Phillips et al.* [2008]. *Eidhammer et al.* [2010] published a revision of the $\Omega_{X,1,*}$ value for dust, changing it from 5.0×10^{-7} m^2 kg^{-1} to 2.0×10^{-6} m^2 kg^{-1}. Using the new value would predict fewer ice nuclei from dust because the denominator is larger in equation (2). The size limit of 0.1 μm is supported by measurements of snow residuals [*Pruppacher and Klett*, 1997; *Chen et al.*, 1998; *Prenni et al.*, 2007; *Marcolli et al.*, 2007]. The parameter α_X is the fractional contribution from aerosol group X to the IN concentration which was inferred from several field campaigns. Dust contributes 2/3, and BC/OM contributes 1/3. For BC/OM, the contribution from the organic matter (OM) is assumed to be 0.06, based on the assumption (made by *Phillips et al.* [2008]) that half of the residual organic aerosol particles sampled from ice crystals (which is 13%) [*Targino et al.*, 2006; *DeMott et al.*, 2003; *Cziczo et al.*, 2004; *Richardson et al.*, 2007; *Phillips et al.*, 2008] are ice nuclei. Please note that there are significant uncertainties associated with the use of this assumption. The contribution from BC for the reference condition in the *Phillips et al.* [2008] parameterization is therefore assigned the value of 1/3–0.06.

[15] H_X, is a factor that ranges from 0 to 1, and represents the relative scarcity of nucleation seen at relative humidities well below water saturation at temperatures warmer than −40°C. Here, since we assume water saturation during ice formation for all mixed phase clouds, Hx = 1 for all chemical compositions. The value of $\xi(T)$ in equation (2) is zero at T > −2°C, and 1 for T < −5°C, and interpolated in between, in order to account for the fact that no droplets freeze at

Table 1. Description of Parameters Used in This Paper

Parameter	Description	Value and Units
a	Parameter used in Meyers parameterization	−0.639
b	Parameter used in Meyers parameterization	0.1296
C_c	Cunningham correction factor	
D	Vertical decay rate in Meyers parameterization	
D_{cnt}	Brownian aerosol diffusivity	$m^2\ s^{-1}$
D_X	Geometric mean diameter of aerosol in group X for X = {Dust, BC/OM}	μm
H_X	Fraction-reducing IN activity at low S_i, warm T	
IN_{CON}	Ice nuclei number concentration for contact freezing	m^{-3}
$IN_{CON,X}$	Ice nuclei number concentration for contact freezing from group X for X = {Dust, BC/OM}	m^{-3}
IN_{DCI}	Ice nuclei number concentration for immersion/condensation freezing	L^{-1}
$IN_{DCI,X}$	Ice nuclei number concentration for immersion/condensation freezing from group X for X = {Dust, BC/OM}	kg^{-1}
$J_{frz,cnt}$	Ice Number increase rate from contact freezing	$10^{12}\ kg^{-1}\ s^{-1}$
k_B	Boltzmann constant	1.381×10^{-23}
$n_{IN,1,*}$	Number mixing ratio of reference activity spectrum for water saturation in background troposphere scenario	kg^{-1}
n_X	Number mixing ratio of particles in aerosol group X	kg^{-1}
N_{a0}	Number concentration of active ice nuclei at −4°C	m^{-3}
N_d	Number concentration of cloud droplets	$10^{12}\ kg^{-1}$
r_{cnt}	Number mean radius of aerosols	m
r_v	Volume mean radius of droplets	m
S_i	Saturation ratio of vapor with respect to ice	
S_i^w	Value of S_i at water saturation	
T	Physical temperature of ambient air in °C	°C
T_k	Physical temperature of ambient air in kelvin	K
ΔT_{CIN}	Difference in freezing temperature between surface and bulk water modes	4.5°C
X	Label for group of insoluble aerosol	
α_X	Fraction of $n_{IN,1,*}$ (H_X = 1) from IN activity of group X = {Dust, BC/OM}	{2/3, 1/3 − 0.06}
z	Altitude	m
μ	Viscosity of air	$kg\ m^{-1}\ s^{-1}$
μ_X	Average number of ice embryos per aerosol particle in group X	
ρ_0	Density of ambient air	$kg\ m^{-3}$
$\xi(T)$	Function that is 0 for $T > -2$°C and 1 for $T < -5$°C, being δ_0^1 (T, −5, −2) for −5 < T < −2°C	
Ω_X	Total surface area of all aerosols larger than 0.1 μm in diameter from group X	[aerosol] m^2 [air] kg^{-1}
$\Omega_{X,int}$	Interstitial component of Ω_X	[aerosol] m^2 [air] kg^{-1}
$\Omega_{X,1,*}$	Component of Ω_X in background troposphere scenario for aerosol diameters between 0.1 and 1 μm with X = {Dust, BC/OM}	[aerosol] m^2 [air] kg^{-1}

temperatures higher than −2°C. At conditions with low ice freezing fractions, $\mu_X \ll 1$, we have

$$IN_{DCI,X} \approx H_X(S_i,T)\xi(T)\left(\frac{\alpha_X n_{IN,1,*}}{\Omega_{X,1,*}}\right)\Omega_X \quad (3)$$

Therefore, the ice nuclei concentrations from each group of aerosols are based on their contribution to the ice nuclei measurements at the reference condition, which are then adjusted by the calculated aerosol surface area concentration, temperature, and ice supersaturation to account for regional and seasonal variations.

2.2.1.2. The Meyers Parameterization

[16] The Meyers parameterization has been used in both global and cloud resolving models [*Gettelman et al.*, 2010; *Lee and Penner*, 2010; *Muhlbauer et al.*, 2010; *Salzmann et al.*, 2010]. The number concentration of ice nuclei as a function of ice supersaturation (S_i) is formulated as

$$IN_{DCI} = \exp\{a + b[100(S_i - 1)]\}D \quad (4)$$

$$D = \begin{cases} 1.0 & (z \le 1000\ m) \\ 10^{-(z-1000)/6700} & (1000\ m < z \le 7000\ m) \\ 10^{-6000/6700} & (z > 7000\ m) \end{cases} \quad (5)$$

where $a = -0.639$ and $b = 0.1296$. The vertical decay rate (D) [*Liu et al.*, 2007] is based on the measured vertical profiles of nonvolatile particle number concentrations in the Northern Hemisphere at midlatitudes during the INCA campaign [*Minikin et al.*, 2003] and accounts for the fact that the original Meyers formulation was based on surface measurements. It is about tenfold per 6.7 km from the boundary layer top to 7 km with no variation above 7 km. Note that the Meyers parameterization is not dependent on aerosol characteristics, but only on supersaturation with respect to ice.

2.2.2. Contact Freezing

[17] The contact freezing of cloud droplets is thought to occur through Brownian coagulation with insoluble IN. The production rate of ice number from contact freezing is based on the work by *Liu et al.* [2007]:

$$J_{frz,cnt} = 4\pi r_v N_d IN_{CON} D_{cnt}/\rho_0 \quad (6)$$

where r_v is the volume mean droplet radius, N_d the number concentration of cloud droplets, and ρ_0 the air density. D_{cnt} is the Brownian aerosol diffusivity, and is calculated as:

$$D_{cnt} = \frac{k_B T_k C_c}{6\pi\mu r_{cnt}} \quad (7)$$

where T_k is the physical temperature of ambient air in Kelvin, r_{cnt} is the aerosol number mean radius, C_c the Cunningham correction factor, k_B the Boltzmann constant, and μ the viscosity of air. The number concentration of contact IN, IN_{CON} is parameterized using either the Phillips contact IN parameterization or the Young contact IN parameterization.

2.2.2.1. The Phillips Contact IN Parameterization

[18] *Phillips et al.* [2008] proposed treating contact IN using the same representation as that for the immersion or condensation nuclei, but assuming that the contact freezing temperature of the same particle is 4.5°C higher than the immersion and condensation nucleation temperature, based on measurements by *Shaw et al.* [2005]. However, it should be noted that *Shaw et al.* [2005] used volcanic ash aerosol particles that were100–300 μm in size, which is larger than the size of most aerosol particles at mixed phase cloud altitudes. Nevertheless, if freezing is a surface phenomena, and we make the assumption that the number of active sites is proportional to the particle surface area, then the freezing with a submicrometer particle inside the drop would be much less efficient than that with a particle of 100–300 μm size. However, contact freezing with the particle at the surface of the drop will probably be less affected by the size of the particle due to the limited area of contact with the drop surface. Therefore, the difference between the surface mode and bulk water mode for submicrometer particles will probably be at least as large as that observed by *Shaw et al.* [2005], so we adopt the 4.5°C change in freezing temperature here. The number mixing ratio of potentially active contact IN is represented by

$$\mathrm{IN}_{CON,X} \cong \alpha_X \xi(T) \left\{ \frac{n_{\mathrm{IN},1,*}\left[T - \Delta T_{CIN}, S_i^w (T - \Delta T_{CIN})\right]}{\Omega_{X,1,*}} \right\} \Omega_{X,\mathrm{int}} \tag{8}$$

$\Omega_{X,\mathrm{int}}$ is the component of Ω_X for interstitial IN and S_i^w is the value of ice saturation ratio at water saturation. The Phillips contact freezing parameterization thus preserves the surface area dependence of the Phillips DCI freezing parameterization.

[19] In the current setup, all of the three processes that remove aerosols from the interstitial phase (droplet nucleation, contact freezing, DCI freezing) are assumed to occur simultaneously, and the cloud droplet number and ice number formed during the time step are based on the number of aerosol particles at the beginning of the present time step. Whether the cloud droplet number (or ice crystal number from DCI freezing) increases at the end of the time step depends on the difference between the cloud droplet number (or ice crystal number from DCI freezing) formed during this time step and the previous time step [*Liu et al.*, 2007, equation (4)]. While it may be tempting to exclude the aerosols that are predicted to activate as CCN or DCI freezing nuclei during the current time step from being contact ice nuclei, this would be inaccurate, because it assumes that CCN or DCI activation always occurs prior to contact nucleation. Also the droplet number or ice crystal number from DCI freezing does not increase until the end of the time step. Furthermore, the GCM we use does not presently carry information about the contributions from different aerosol species to the droplet number increase at the current time step. A more appropriate method would be to carry a separate "interstitial" group for each of the aerosol species. However, doing so requires a substantial amount of work and would significantly increase the computer time associated with the model, so that adding this capability was beyond the scope of the present study. Thus, here we assume that all aerosols are interstitial and $\Omega_{X,int} = \Omega_X$. We nevertheless acknowledge that this may result in an over estimation of the Phillips contact freezing.

2.2.2.2. The Young Contact IN Parameterization

[20] The Young parameterization for contact nuclei is

$$\mathrm{IN}_{CON} = N_{a0}(270.16 - T_k)^{1.3} \tag{9}$$

where N_{a0} is the number concentration of active ice nuclei at -4°C, which was determined to be 0.2 cm^{-3} by *Young* [1974]. However, this assumption cannot be used without adjustment, since it does not allow for regional differences in contact ice nuclei due to aerosol abundance, and cannot be used to study aerosol effects on mixed phase clouds. Several studies have attempted to introduce aerosol dependence into contact freezing parameterizations by making various assumptions. *Liu et al.* [2007] assumed that all dust aerosols act as contact ice nuclei. *Gettelman et al.* [2010] assumed that only coarse mode dust aerosols were contact ice nuclei. *Lohmann* [2002] made several assumptions: contact ice nuclei were assumed to be all dust aerosols, the dust aerosol mass was reduced by the mass of sulfate aerosol before calculating the contact IN, or all hydrophobic carbonaceous particles were contact IN. *Lohmann and Diehl* [2006] assumed that contact ice nuclei were hydrophilic black carbon and accumulation mode dust aerosols, multiplied by a temperature-dependent fraction. This linear temperature dependence function implies that 100% acts as contact IN at T < -17°C for dust, and at T < -26°C for black carbon. *Storelvmo et al.* [2008] assumed that if dust and BC aerosols were coated with less than one monolayer of soluble material, they would be contact freezing nuclei. Finally, *Lohmann et al.* [2007] assumed externally mixed dust and BC would act as contact freezing nuclei. Here, we assume that all hydrophobic dust and black carbon/organic matter can act as contact IN at -4°C. Furthermore, we assumed that all dust was hydrophobic and that the hydrophobic fraction of BC/OM was 17%, which is the global average value from the general circulation model simulation of *Reddy and Boucher.* [2004]. The justification for BC/OM acting as contact ice nuclei is given by *Pruppacher and Klett* [1997], who state that organic compounds as well as other compounds are considerably better IN when acting in the contact mode rather than in the freezing or deposition modes. In addition, *Gorbunov et al.* [2001] found that soot particles act as efficient ice nuclei and their result has been interpreted as contact freezing, though this is under debate [*Storelvmo et al.*, 2008]. Therefore, N_{a0} is given as the sum of the number concentration of dust and 17% of the number concentration of black carbon/organic matter. Assuming all hydrophobic dust and BC/OM as contact IN might be an overestimation. In section 3.9, we discuss a sensitivity simulation, where the percentage of dust and BC/OM that act as contact ice nuclei is greatly reduced to match the contact IN concentration (0.2 cm^{-3}) assumed by *Young* [1974]. The

Table 2. Sensitivity Simulations

Simulation	Description
Mey_YCT	Reference simulation using *Meyers et al.* [1992] parameterization for DCI freezing and *Young* [1974] parameterization for contact freezing
Phi_YCT	*Phillips et al.* [2008] parameterization for DCI freezing and *Young* [1974] parameterization for contact freezing
Mey_PCT	*Meyers et al.* [1992] parameterization for DCI freezing and *Phillips et al.* [2008] parameterization for contact freezing
Phi_PCT	*Phillips et al.* [2008] parameterization for DCI freezing and *Phillips et al.* [2008] parameterization for contact freezing
Phi_PCT_PImix	Same as Phi_PCT but with preindustrial black carbon and organic matter for mixed phase clouds ice nucleation
Phi_YCT_PImix	Same as Phi_YCT but with preindustrial black carbon and organic matter for mixed phase clouds ice nucleation
Phi_YCT_Less	Same as Phi_YCT but with a reduced fraction of BC/OM and dust as contact IN to match the original *Young* [1974] assumption

impact to the anthropogenic aerosol forcing in mixed phase clouds is also discussed there.

2.3. Setup of Simulations and Experimental Design

[21] We use 26 vertical levels and a horizontal resolution of $2^\circ \times 2.5^\circ$ for both the CAM3 and IMPACT models in this study. The time step for CAM3 is 30 min, and that for advection in IMPACT is 1 h. The finite volume dynamical core for CAM3 is used.

[22] Six model experiments are designed. Table 2 summarizes the setup of the experiments. The Mey_YCT case employs the Meyers parameterization for DCI IN and the Young parameterization for contact IN, similar to the original setup of the CAM-IMPACT model [*Wang and Penner*, 2010]. Therefore, we specified this as the reference case. Phi_YCT is similar to Mey_YCT, except that the DCI IN parameterization is replaced by the Phillips parameterization. In Mey_PCT and Phi_PCT the contact IN parameterization is that of *Phillips et al.* [2008]. Two preindustrial simulations Phi_PCT_PImix and Mey_PCT_PImix are performed, in order to gauge the overall impact of mixed phase clouds on climate forcing.

[23] All the six experiments were run for 5 years and 4 months with fixed present-day sea surface temperatures. The first 4 months are treated as model spin-up and are excluded from the analysis presented below. Assessments are made of the changes of ice nuclei number concentration, cloud liquid/ice amount, the global radiation budget, and the effect of anthropogenic aerosols in mixed phase clouds.

3. Results and Discussion

3.1. Comparison of Deposition/Condensation/Immersion Ice Nuclei Distributions

[24] Figures 1a, 1b, and 1c show the zonal and annual mean plots of DCI IN predicted in the Mey_YCT and Phi_YCT simulations (Table 2) and their differences. Distinct features are seen using the two different parameterizations. In Mey_YCT, the ice nuclei concentration in the Southern and Northern Hemispheres generally follows the temperature distribution. This is caused by the assumption that mixed phase clouds are at water saturation, so that the ice saturation ratio follows the temperature distribution. However, in Phi_YCT, there is a peak in the DCI IN concentrations near 400 hPa at 60° latitude in both hemispheres, with the peak in the Northern Hemisphere larger than that in the Southern Hemisphere. The peak in the DCI IN concentration can be attributed to the combined effects of the aerosol availability and the temperature that is most suitable for producing DCI IN, which can be shown by comparing with the aerosol distributions (Figures 1d, 1e, and 1f) and the temperature distribution (not shown). The larger peak in the Northern Hemisphere is due to the larger aerosol concentrations in the Northern Hemisphere.

[25] One can also notice that there is a "pipeline" of DCI IN near 40°N from the surface up toward the middle troposphere, which may correspond to the upward transport of dust from eastern China/Mongolia and BC/OM from Northern Hemisphere (NH) industrial regions (Figure 2). This is consistent with the hypothesis proposed by *Isono et al.* [1970] and *Hobbs et al.* [1971a, 1971b] that the dust storms in northern China and Mongolia can be advected by strong tropospheric winds and create an IN storm. The region above the equator is found to be deficient in IN which is similar to the summary given by *Pruppacher and Klett* [1997]. The other two cases, Phi_PCT and Mey_PCT show similar features in the predicted DCI IN concentrations, so their figures are not included here. In the Southern Hemisphere (SH), the Phillips DCI freezing parameterization generally produces smaller DCI IN concentrations than the Meyers parameterization (see Figure 1c). In the NH, the Phillips DCI freezing parameterization produces larger DCI IN concentrations than the Meyers parameterization at altitudes around 400∼600 hPa. At lower altitudes in the NH, the relative differences between the two parameterizations depend on latitude. Between 30°N and 60°N, due to higher aerosol concentrations, the DCI IN concentration predicted by the Phillips DCI freezing parameterization is larger than that from the Meyers parameterization. However, from 60°N onward, the Meyers parameterization predicts larger DCI IN concentration than the Phillips DCI freezing parameterization.

[26] Figures 2a and 2b show the horizontal distribution of the vertically integrated DCI ice nuclei concentration for the Mey_YCT and Phi_YCT simulations. The simulation Phi_YCT shows a clear north-south contrast in the DCI IN concentration distribution patterns, which is not present in the Mey_YCT simulation. This north-south contrast is due to the differences in the aerosol distributions between the two hemispheres (see Figures 2d, 2e, and 2f). The maxima of the DCI IN concentration in the Phi_YCT simulation is above the eastern China/Mongolia region, due to the high concentration of dust aerosol and the low temperatures there. Dust emissions from the Saharan desert and Australia are clearly seen in the DCI IN predicted from Phi_YCT. Fossil fuel burning BC/OM in the industrialized regions of southeast Asia, Europe, and North America; biomass burning BC/OM in South America and middle Africa do not have a significant impact on the distribution of DCI IN,

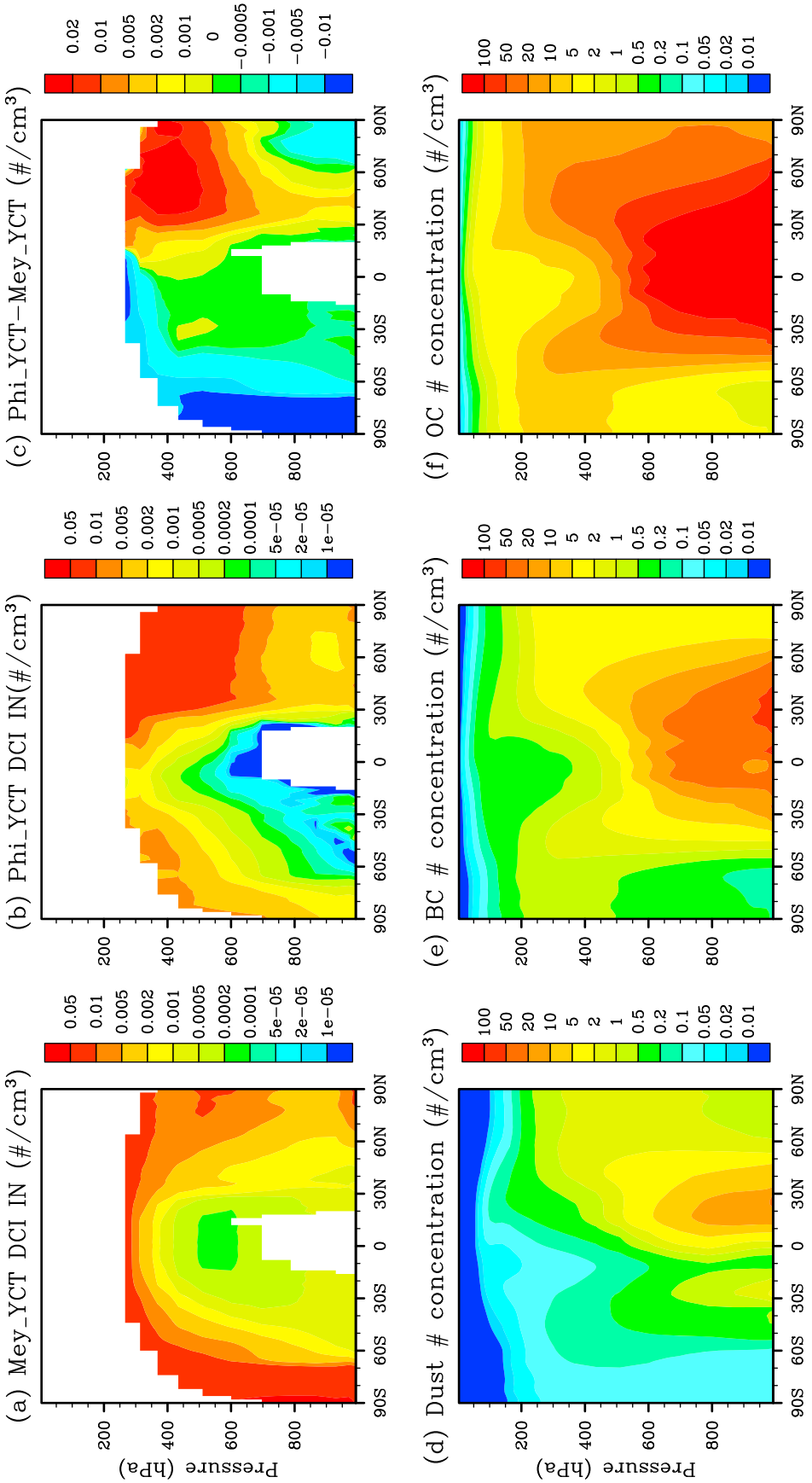

Figure 1. (a, b, and c) Zonal and annual mean latitude versus pressure plots of deposition/condensation/immersion freezing ice nuclei in Mey_YCT, Phi_YCT, and their differences. (d, e, and f) Zonal and annual mean latitude versus pressure plots of dust, black carbon, and organic carbon.

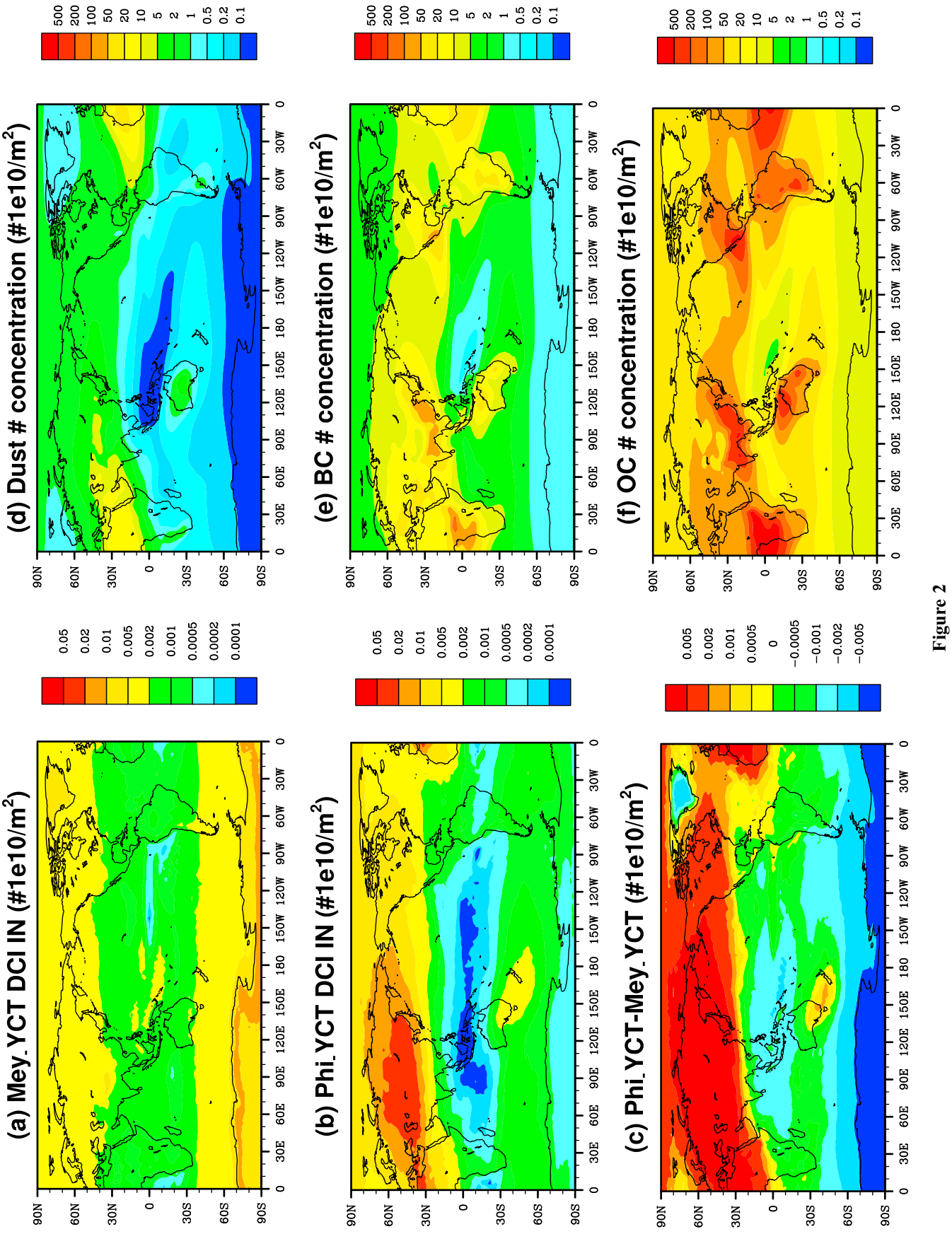
(a) Mey_YCT DCI IN (#1e10/m2)
(b) Phi_YCT DCI IN (#1e10/m2)
(c) Phi_YCT-Mey_YCT (#1e10/m2)
(d) Dust # concentration (#1e10/m2)
(e) BC # concentration (#1e10/m2)
(f) OC # concentration (#1e10/m2)
90N 60N 30N 0 30S 60S 90S
0 30E 60E 90E 120E 150E 180 150W 120W 90W 60W 30W 0
0.05 0.02 0.01 0.005 0.002 0.001 0.0005 0.0002 0.0001
0.005 0.002 0.001 0.0005 0 −0.0005 −0.001 −0.002 −0.005
500 200 100 50 20 10 5 2 1 0.5 0.2 0.1

Figure 2

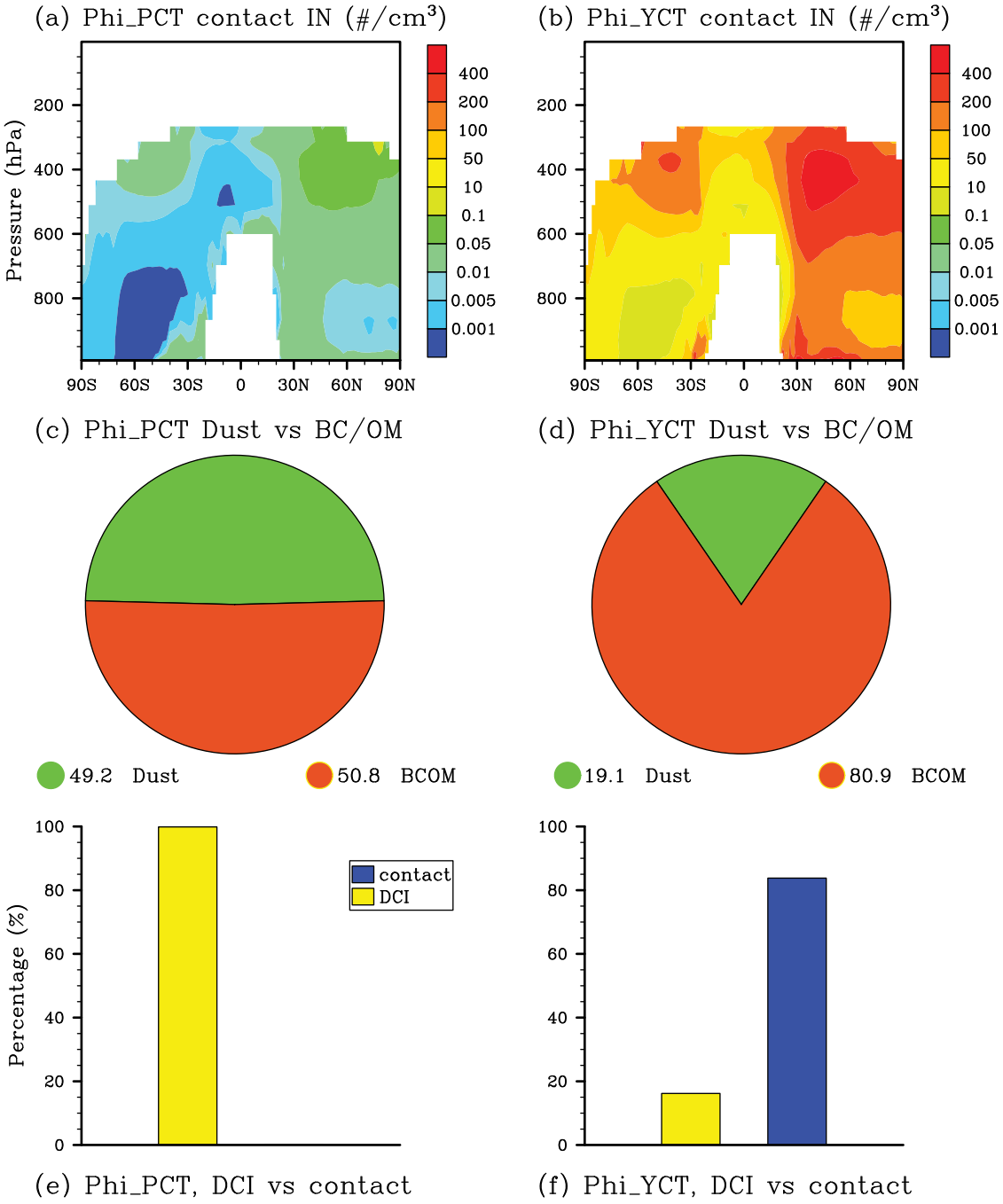

Figure 3. Zonal and annual mean latitude versus pressure plots of contact freezing ice nuclei for the (a) Phi_PCT simulation and the (b) Phi_YCT simulation. (c and d) Global and annual average fraction of dust and BC/OM contact IN in mixed phase clouds for the two simulations and (e and f) global and annual average relative contribution of contact freezing and DCI freezing to newly formed ice crystals.

because BC and OM together contribute only about 1/3 of the total DCI IN in the Phillips parameterization. In general, the DCI ice nuclei distribution predicted by Phi_YCT is larger in regions with higher aerosol emissions, and vice versa. Whereas the Meyers parameterization only tends to increase with decreasing temperature and does not include, for example, variations associated with dust. In sections 3.2–3.8, we discuss how the correlation of the IN concentrations

Figure 2. (a, b, and c) Vertically integrated latitude versus longitude plots of annually averaged deposition/condensation/immersion freezing ice nuclei in Mey_YCT and Phi_YCT, and their differences. (d, e, and f) Vertically integrated annually averaged latitude versus longitude plots of dust, black carbon, and organic carbon.

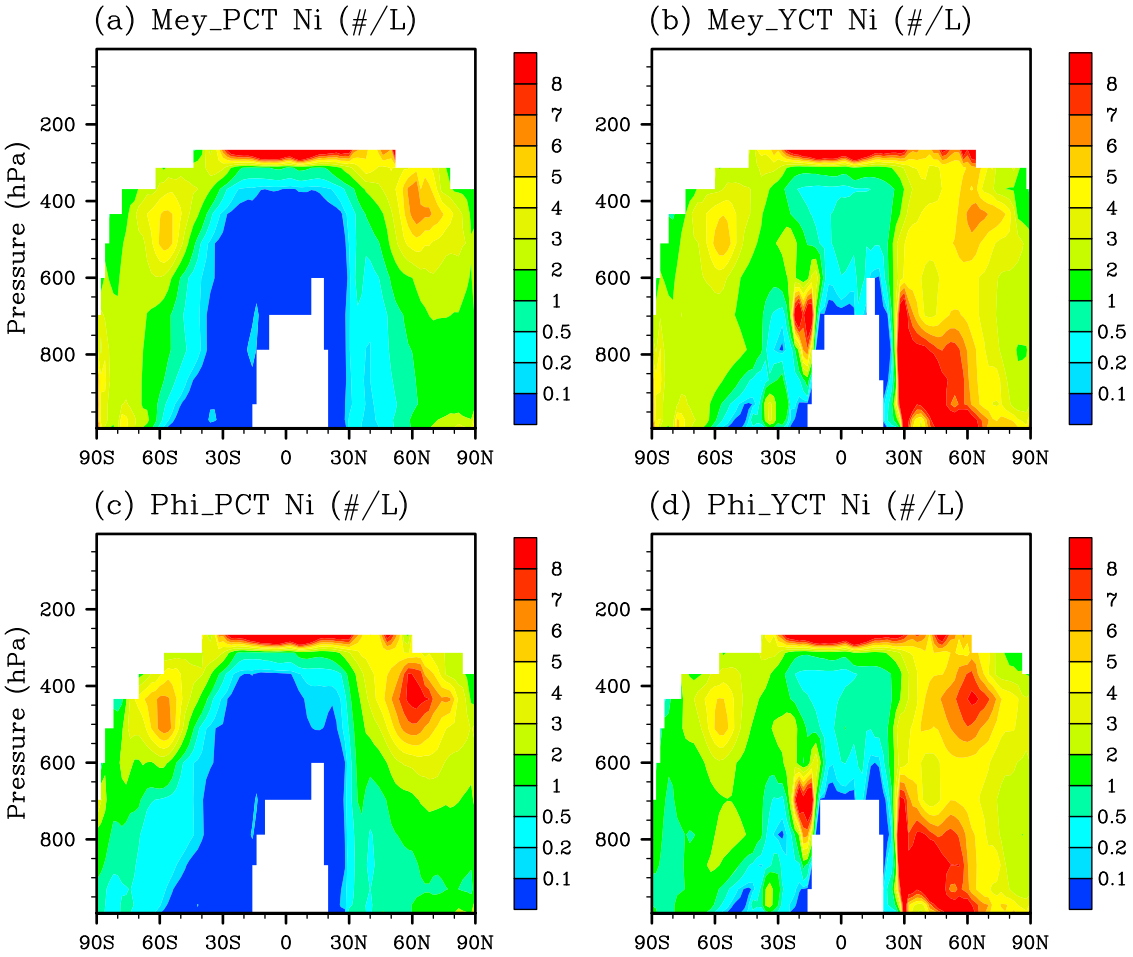

Figure 4. Zonal and annual mean latitude versus pressure plots of ice crystal number concentration in mixed phase clouds from the four simulations.

with the aerosol fields in the simulations using Phillips DCI freezing parameterization changes the spatial variations of the cloud ice field, the cloud fractions, and the global radiation budget.

3.2. Comparison of Contact Ice Nuclei Distributions

[27] Figures 3a and 3b show the contact IN predicted by the Phi_PCT and Phi_YCT cases. The contact IN predicted by Mey_PCT and Mey_YCT are not shown because they are very similar to the Phi_PCT and Phi_YCT cases. As shown in Figure 3, using the Phillips contact freezing parameterization decreases the contact IN concentration by 3 orders of magnitude. The spatial distribution of contact IN predicted from the two parameterizations is, however, very similar. There are two peaks of contact IN number concentrations around 400 hPa at midlatitudes of both hemispheres, with the peak in the NH larger than that in the SH. The number concentration and spatial distribution of contact IN in the YCT cases are very similar to those shown by *Lohmann* [2002] in which the contact nuclei are assumed to be insoluble carbonaceous particles (sum of hydrophobic black carbon and organic carbon). Figures 3c and 3d show the percentage contribution from dust and BC/OM to the contact ice nuclei predicted from the two cases. For the Phi_PCT case, the contributions from dust and BC/OM are relatively equal, while for the Phi_YCT case, the contribution from BC/OM is much larger than that from dust. The reason is that the Phillips contact freezing parameterization prescribes the fractional contribution of dust to total ice nuclei at the reference condition to be 2/3 and the fractional contribution of BC/OM to be 1/3. Thus, even though the BC/OM surface and number concentrations are much larger than those of dust, the contribution from dust remains large. Figures 3e and 3f compare the relative contribution of contact freezing and DCI freezing to newly formed ice crystals. The contribution of contact freezing is minimal in the Phi_PCT case, with DCI freezing contributing almost 100%. However, in the Phi_YCT case, contact freezing contributes more than DCI freezing, with the relative contribution of the two being 83.81% and 16.19%, respectively.

3.3. Zonal Mean Latitude-Pressure Cross Sections of Ice and Liquid Cloud Properties in Mixed Phase Clouds

[28] Figure 4 shows zonal and annual average plots of the grid average ice crystal number concentrations (Ni) in mixed phase clouds from the four present-day simulations. A comparison of Mey_PCT with Phi_PCT, and of Mey_YCT with Phi_YCT shows that the use of the Phillips DCI freezing parameterization predicts more ice crystals in the middle troposphere of the NH, and fewer ice crystals in

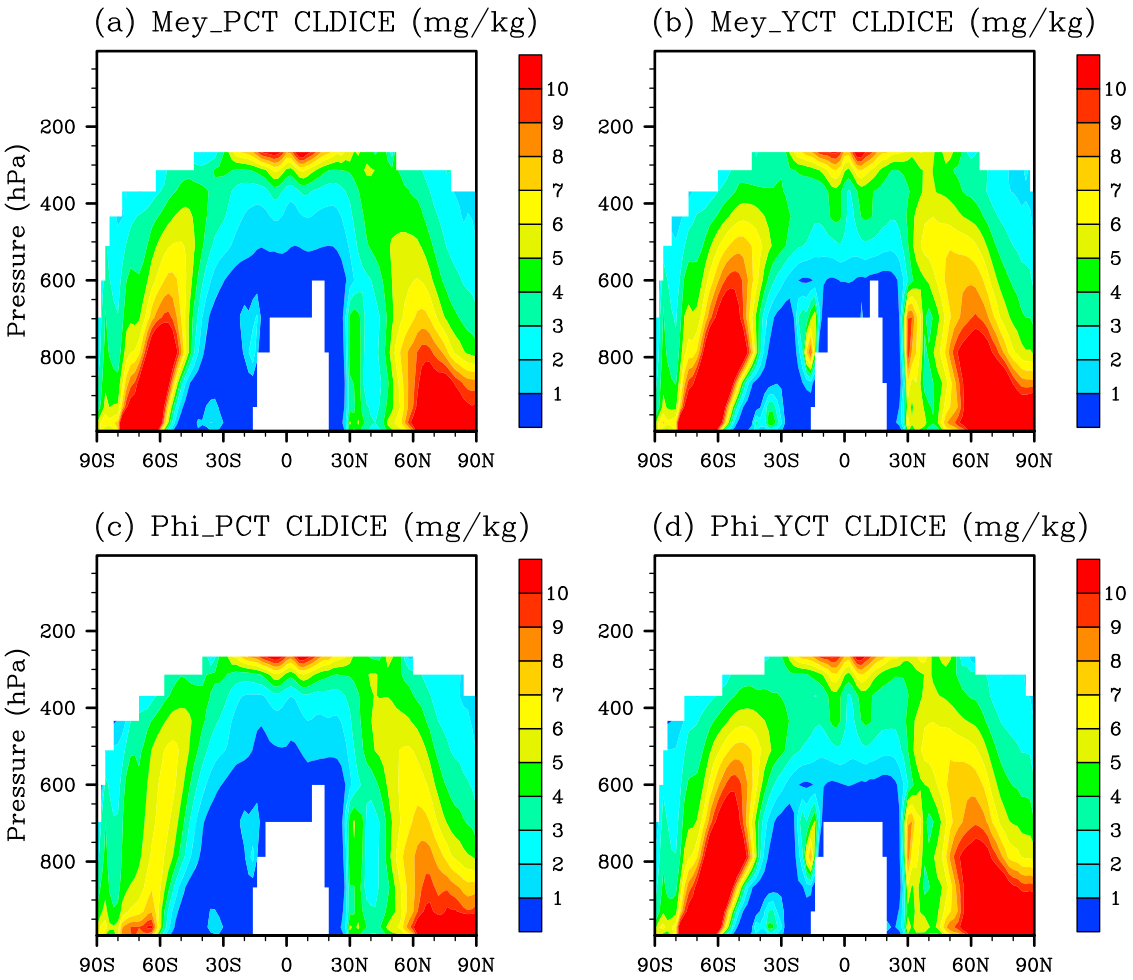

Figure 5. Zonal and annual mean latitude versus pressure plots of ice water mixing ratio in mixed phase clouds from the four simulations.

almost all of the SH. This is consistent with the comparison of the DCI ice nuclei distributions. Where ice crystal number concentrations increase, the effective ice crystal radius decreases and vice versa (figure not shown), because the limitation of the available water vapor will hinder the growth of the more numerous ice crystals. This is consistent with the findings of *Storelvmo et al.* [2011]. In addition, we expect that smaller ice crystal sizes decrease gravitational settling and lead to longer cloud lifetimes and larger ice water mixing ratios. This is demonstrated by the increase in ice water mixing ratio between 400 hPa and 600 hPa in the NH and the decrease in ice water mixing ratio in the SH with the Phi cases compared to the Mey cases (Figure 5). At the same subfreezing temperature, the saturation vapor pressure over ice is smaller than that over water. Therefore, water vapor will condense onto existing ice crystals, while liquid droplets will evaporate to compensate for the depleted water vapor. This is the so-called Bergeron-Findeisen process. In places where we see an increase in ice water and ice number, the radius of cloud droplets is decreased (Figure 6), and vice versa, because of the stronger Bergeron-Findeisen process. For example, the cloud droplet effective radius is smaller in Phi_PCT than in Mey_PCT in the NH between 400 and 600 hPa, and larger in the SH. The change in the cloud droplet effective radius in the NH between Mey_YCT and Phi_YCT is not very apparent because of the dominant effect of the Young contact freezing parameterization (Figure 3f). Droplet evaporation in the model is represented by assuming that the loss rate of cloud liquid droplet number from the Bergeron-Findeisen process is half of the loss rate of the cloud liquid mass in the model. The changes of cloud droplet number and cloud liquid water mixing ratio are similar to that of the cloud droplet radius in these regions (figures not shown).

[29] The Young contact freezing parameterization predicts more ice crystals at all latitudes and heights than does the Phillips contact freezing parameterization (Figure 4). Although the number concentration of contact ice nuclei decreases by 3 orders of magnitude from the YCT to the PCT cases (compare Figure 3a to Figure 3b), the number concentration of ice crystals changes by less than 1 order of magnitude (compare Figure 4a to Figure 4b, or Figure 4c to Figure 4d). This is because the contact freezing rate also depends on the number concentration of cloud droplets, which is larger in the PCT cases where contact freezing is less efficient, and thus has a buffering effect on the change of contact freezing rate. This buffering effect was also pointed out by *Lohmann* [2002]. The ice crystal number

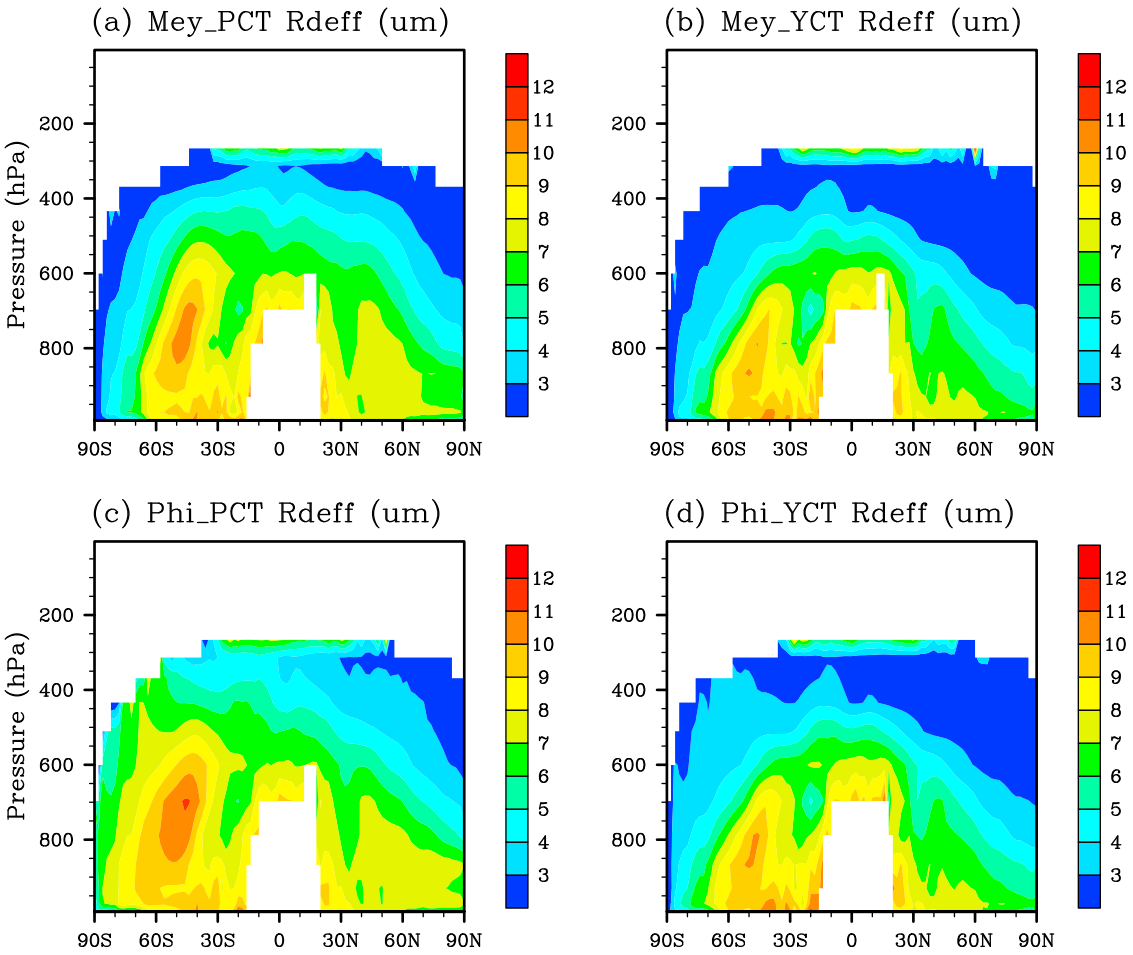

Figure 6. Zonal and annual mean latitude versus pressure plots of effective cloud droplet radius in mixed phase clouds from the four simulations.

concentration is significantly larger in the YCT cases in the region below 800 hPa at NH midlatitudes (between 30°N and 60°N). This is probably associated with fossil fuel BC and OM emissions in this region. *Lohmann* [2002] showed a similar increase between a case where contact ice nuclei was assumed to be both dust and black carbon and a case where only dust acted as contact nuclei [*Lohmann*, 2002, Figure 3]. The larger ice crystal number concentration in the YCT cases leads to smaller effective ice crystal radii and higher cloud ice water mixing ratios. For example, the cloud ice water mixing ratio is larger in the Phi_YCT simulation (Figure 5d) than in the Phi_PCT simulation (Figure 5c). Because of the more efficient Bergeron-Findeisen process, the effective droplet radius (Figure 6), droplet number concentration, and cloud liquid content are smaller in all regions in the YCT cases. Overall, the effect of changing the contact freezing parameterization from Young to Phillips on the cloud liquid and ice field is more pronounced than that of changing the DCI parameterization from Meyers to Phillips.

3.4. Probability Distributions of In-Cloud Ice Fraction

[30] Figure 7 shows the probability distributions of in-cloud ice fraction (in-cloud ice water content divided by in-cloud total water content) in different temperature ranges from the four present-day simulations as well as observations from *Korolev et al.* [2003]. Model output is calculated in the same way as described by *Gettelman et al.* [2010]. Ice fraction is calculated only for grid points in mixed phase conditions between 1000 and 100 hPa and 90°S and 90°N. All four of the simulations show a high probability of pure liquid and ice cloud conditions and a low probability for mixed phase clouds. The probability distributions of ice fraction for all temperature intervals shift toward lower ice fractions when going from the Mey_PCT case to the Phi_PCT case. There is also a decrease in the frequency of occurrence of intermediate ice fractions. This means, when using the Phillips DCI freezing parameterization, the possibility for a given grid box to have a low ice fraction and high liquid fraction is increased, while the chance of having a mixture of ice and liquid is decreased. Since the model output is calculated from grid boxes ranging from −90° to 90° latitudes, this change in the in-cloud ice fraction is an average result from local changes in cloud ice mass mixing ratio and cloud liquid mass mixing ratio. The differences between the Mey_YCT and Phi_YCT cases are very small because of the dominant effect of contact freezing (Figure 3f).

[31] Comparison of the Phillips contact freezing parameterization to the Young contact freezing parameterization

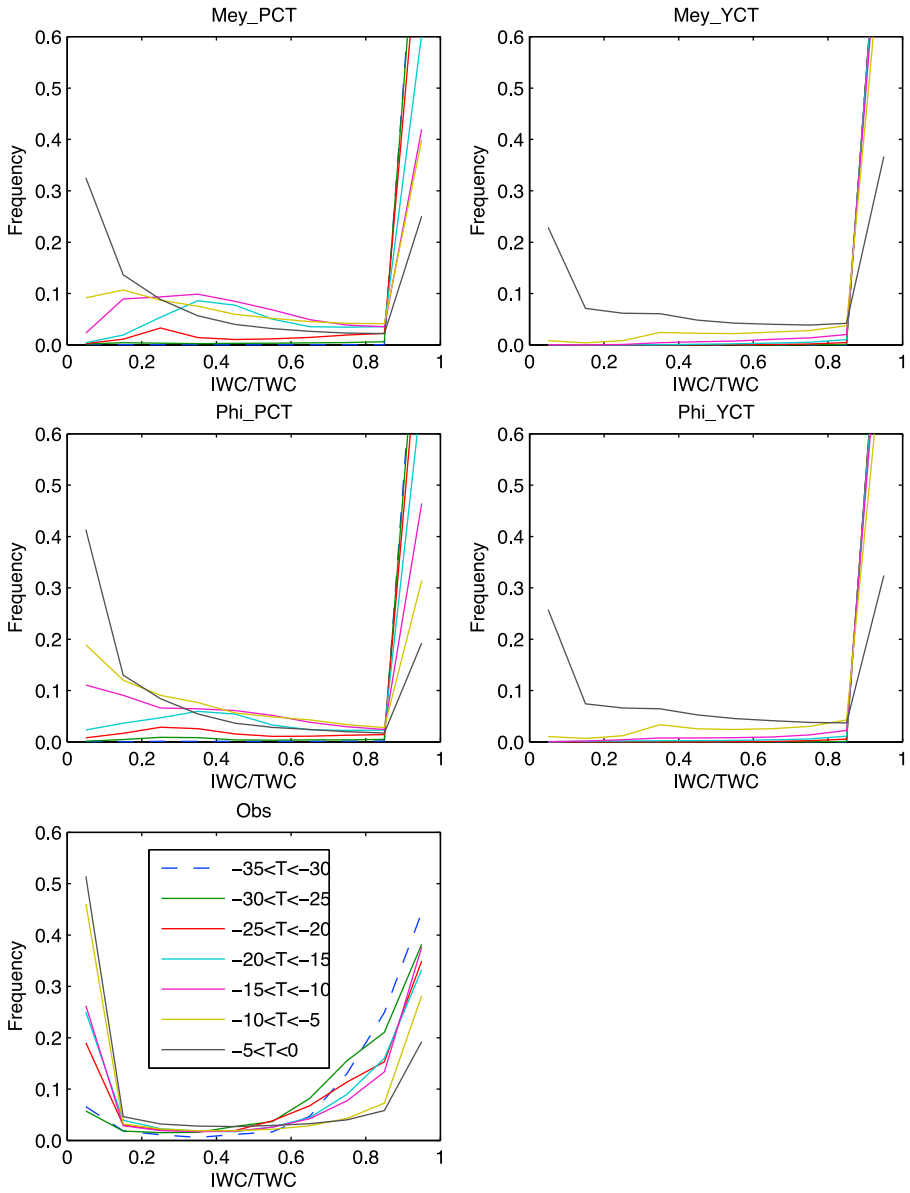

Figure 7. (top and middle) Probability distributions of ice fraction at different temperature ranges predicted by the four present-day simulations. (bottom) Observations from *Korolev et al.* [2003].

(Mey_PCT versus Mey_YCT, and Phi_PCT versus Phi_YCT) shows that there is a significant change in the probability distribution of ice fractions. At all temperatures, the probability is decreased for low and intermediate ice fractions and increased for high ice fractions in the simulations using the Young parameterization. This means, for any given grid box, that there is a higher probability that it contains pure ice cloud than a mixed phase or a supercooled liquid cloud when using the Young contact freezing parameterization. This result is consistent with the larger grid mean ice mass mixing ratio and smaller grid mean liquid mass mixing ratio from the YCT cases compared to the PCT cases (section 3.3). The above changes to the probability distribution of ice fractions will have an effect on the cloud optical depth observed for middle altitudes clouds and therefore affect the cloud fraction comparison to ISCCP observations (discussed in section 3.5).

[32] The frequency of occurrence of nearly pure liquid clouds is too low for all simulations compared to the observations, while the frequency of occurrence of mixed phase conditions is high compared to observations. This might be due to the treatment of vapor deposition to ice simultaneously with the Bergeron-Findeisen process in the model, because the net loss of vapor to ice should only occur when liquid water is used up and saturation with respect to water can no longer be maintained. The current treatment might lead to more cloud ice, which in turn leads to a stronger depletion of cloud liquid by the Bergeron-Findeisen process. An adjustment of the scheme to account for the complete removal of liquid water prior to vapor deposition might improve the comparison. Under the current setup, the Phi_PCT simulation is closer to the observations than the other three cases.

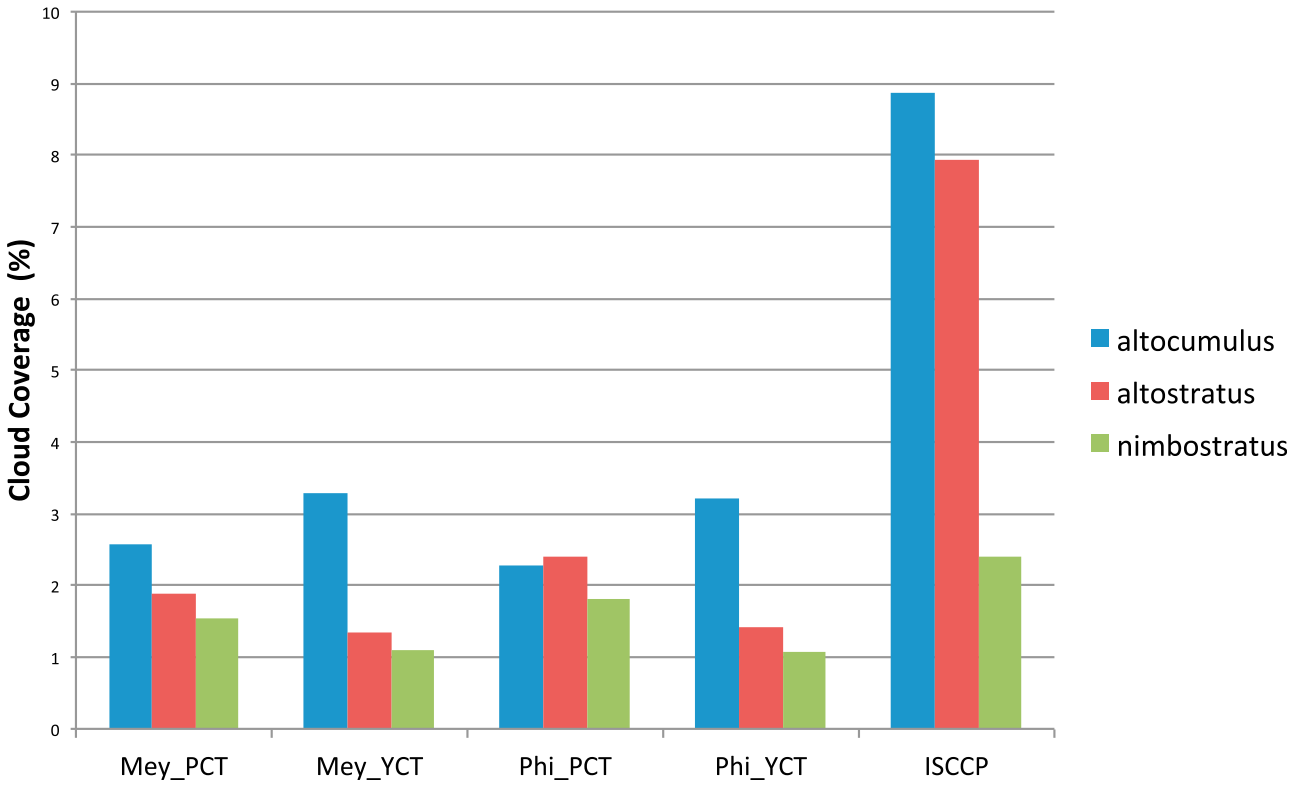

Figure 8. Middle cloud (altocumulus, altostratus, and nimbostratus) fraction (%) predicted from the four simulations and observed in ISCCP.

3.5. Comparison of Middle Cloud Fractions to ISCCP Observations

[33] Figure 8 compares the amount of middle cloud (%) predicted from the four present-day model simulations to that observed in ISCCP. The model outputs are sampled using the ISCCP cloud simulator (http://cfmip.metoffice.com/ISCCP.html), so as to emulate the scenes observed by the satellites. The cloud type is determined by the combination of cloud optical thickness and cloud top pressure using the same criteria as that for the ISCCP satellite observations. For middle clouds, the cloud top pressure criterion is set to be between 680 and 440 hPa. Within the middle cloud category, altocumulus clouds are assumed to have an optical thickness of 0–3.6, altostratus clouds are assumed to have an optical thickness of 3.6–23, and nimbostratus clouds are assumed to have an optical thickness of 23–379. As shown in Figure 8, all of the four model simulations significantly underpredict the optically thin and intermediate middle clouds (altocumulus and altostratus). There is also an underprediction of the optically thick nimbostratus clouds, but to a lesser extent. *Lin and Zhang* [2004] did similar comparisons between the CAM2 cloud fractions and ISCCP observations. They also found a significant underestimation of middle clouds and proposed that "drier atmosphere in the subsidence regime, and lack of cloud formation in shallow convection scheme" are two possible causes [*Lin and Zhang*, 2004, p. 3310]. Comparing the simulation Mey_PCT and the simulation Phi_PCT shows that the cloud fraction of the optically thin altocumulus clouds is decreased from Mey_PCT to Phi_PCT, while the amount of the optically intermediate altostratus clouds, and the optically thick nimbostratus clouds are increased. The latitude-longitude middle cloud distributions (not shown) show that the increases in altostratus and nimbostratus clouds in the Phi_PCT case mainly occur in the SH. This is where we observed a decrease in the cloud ice mixing ratio (Figure 5), and an increase of cloud liquid mixing ratio in the Phi_PCT case. With the same amount of condensed water, liquid water tends to be smaller and more numerous, and thus optically thicker. So having a smaller ice fraction (Figure 7) and a larger liquid fraction increases the cloud optical thickness in the Phi_PCT simulation. Therefore, more middle clouds will be classified as optically intermediate altostratus and optically thick nimbostratus, and less will fall into the altocumulus group.

[34] The Phillips contact freezing parameterization leads to smaller ice fractions than the Young parameterization (Figure 7). So the optical thickness of middle clouds is larger in the simulations using the Phillips contact freezing parameterization compared to those using the Young parameterization for the same reasons as explained above. Therefore, the amount of optically thin altocumulus clouds is smaller in the PCT cases, and the amount of altostratus and nimbostratus clouds are larger. The use of the Phillips DCI freezing parameterization and contact freezing parameterization improves the agreement of altostratus and nimbostratus clouds with ISCCP, at the expense of the agreement of altocumulus clouds.

3.6. Zonal Means of Radiation and Vertically Integrated Mixed Phase Cloud Properties

[35] Figure 9a shows the zonal average distribution of vertically integrated ice crystal number concentration in

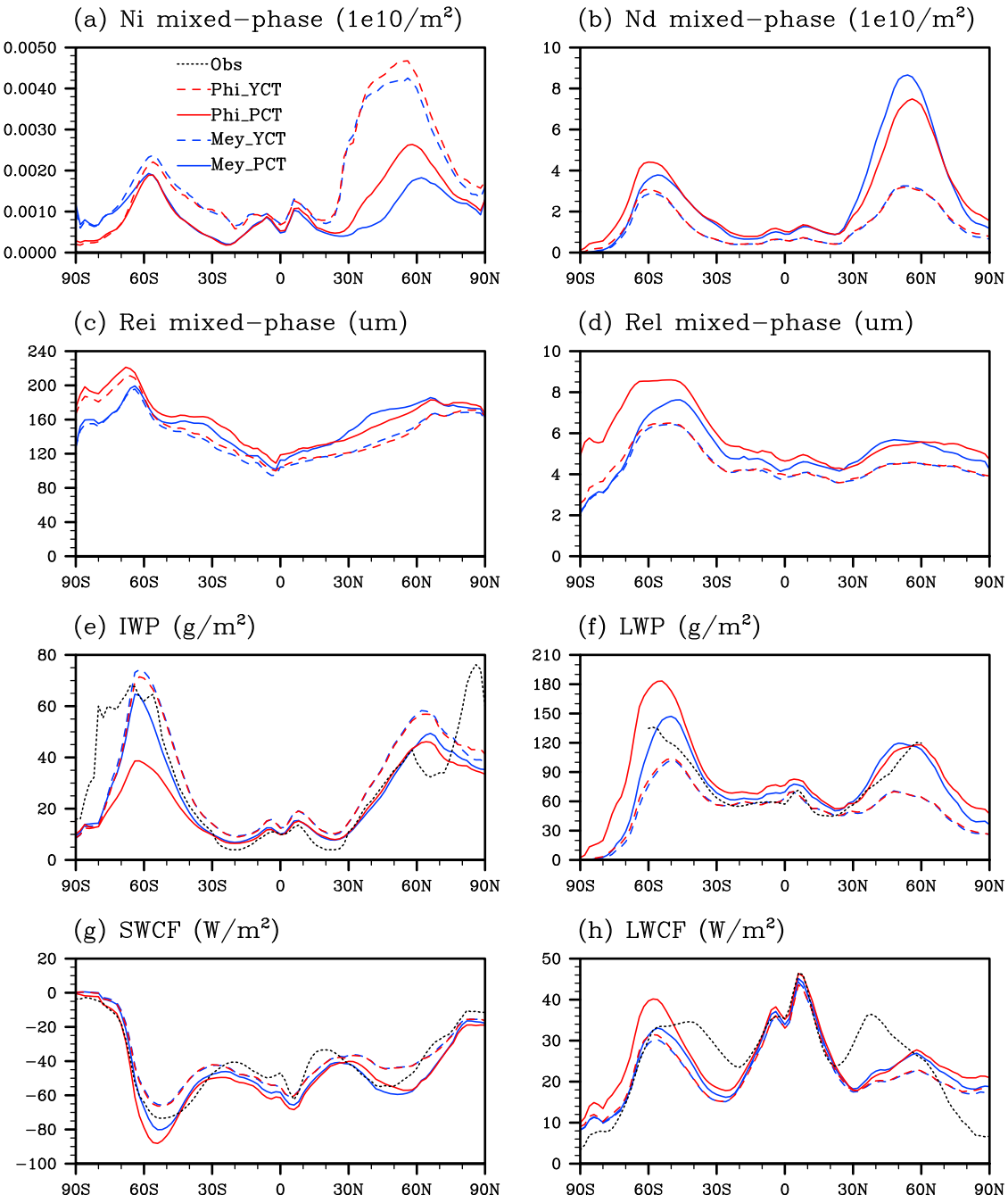

Figure 9. Zonal and annual mean (a) ice crystal number concentration (Ni), (b) vertically integrated mixed phase cloud droplet number concentration (Nd), (c and d) ice crystal radius (Rei) and effective cloud droplet radius (Rel) in mixed phase clouds, (e) ice water path (IWP), (f) liquid water path (LWP), (g) shortwave cloud forcing (SWCF), and (h) longwave cloud forcing (LWCF) from the four present-day model experiments described in Table 2. Black dotted lines refer to CERES data for LWCF and SWCF (http://ceres.larc.nasa.gov), MODIS data for LWP (http://modis.gsfc.nasa.gov/), and ISCCP data for IWP (http://isccp.giss.nasa.gov/).

mixed phase clouds. As anticipated from the latitude-pressure cross section plots, higher ice crystal concentrations occur in cases in which the Young contact freezing parameterization is used, and in cases using the Phillips DCI freezing parameterization in the NH. In the SH, the Meyers parameterization predicts slightly more ice crystals in mixed phase clouds.

[36] The differences in cloud water content and ice crystal number concentration between Mey_YCT and Phi_YCT are small because of the dominant contribution of contact freezing. Therefore, we focus our discussion on the differences between Phi_PCT (red solid line) and Mey_PCT (blue solid line) to reveal the effects of using different DCI

freezing parameterizations. The effective ice crystal radius (Figure 9c) in the Mey_PCT simulation is larger than in the Phi_PCT simulation in the NH midlatitudes, and smaller in the SH due the change in ice crystal number concentration and the limitation of water vapor. The effective cloud droplet radius (Figure 9d) change between Mey_PCT and Phi_PCT is opposite that of the ice crystal number concentration because of the Bergeron-Findeisen process. The smaller ice water path (IWP) in the SH from Phi_PCT compared to that from Mey_PCT leads to more cloud droplets (Figure 9b) and a larger LWP (Figure 9f) because of the less efficient Bergeron-Findeisen process. Since liquid droplets are generally smaller than ice crystals (and because the LWP is larger than the IWP), they tend to produce a larger forcing, so that the shortwave cloud forcing (SWCF) and longwave cloud forcing (LWCF) (defined as the difference in the top-of-atmosphere (TOA) shortwave and longwave radiation between all-sky and clear-sky conditions) are larger in magnitude in Phi_PCT parameterization than in the Mey_PCT parameterization in the SH. It should be noted here that the use of SWCF to evaluate the changes in clouds could also include changes in the surface albedo, which would then be wrongly associated with clouds. However, the top-of-atmosphere clear-sky net solar flux change is only 1.69–5.78% of the top-of-atmosphere full-sky net solar flux change among the model simulations. Since the aerosol field used for different model simulations is very similar, we can assume that the clear-sky net solar flux change mainly comes from clear-sky albedo change. So the effect of clear-sky albedo change on SWCF is small.

[37] *DeMott et al.* [2010] compared a global climate model simulation using the Meyers parameterization and the *DeMott et al.* [2010] IN parameterization that depends both on temperature, and on the number concentration of aerosols exceeding 0.5 μm in diameter. They also observed a decrease in IWP, and increases in LWP, SWCF, and LWCF from the simulation using Meyers to the simulation using the new aerosol-dependent parameterization. The reason for this change was attributed to the reduced IN concentration of nonsea-salt particles larger than 0.5 μm. This is consistent with our finding that the use of the aerosol-dependent IN parameterization decreases IWP, and increases LWP, SWCF, and LWCF.

[38] The Phillips contact freezing parameterization predicts less Ni in mixed phase clouds than the Young contact freezing parameterization. The fewer ice crystals produced using the Phillips contact freezing parameterization leads to larger effective ice crystal radius (compare the red solid line to the red dashed line, and blue solid line to blue dashed line in Figure 9c). It also leaves more water droplets, produces larger effective cloud droplet radius, and LWPs at all latitudes (Figures 9b, 9d, and 9f). Therefore, the SWCF and LWCF are larger in magnitude for the cases that use the Phillips contact freezing parameterization (Figures 9g and 9h).

[39] The global cloud properties predicted by the four present-day model simulations are compared to satellite observations in Figure 9. Since the differences in the SWCF and LWCF field are mainly due to changes in the LWP, which in turn is modified through changes in IWP, we focus our discussion on differences in the IWP here. The IWP data from ISCCP is constructed in the same way as by *Storelvmo et al.* [2008]. Thus, the IWP from 1983 to 2000 from nine cloud types (cirrus, cirrostratus, and deep convective clouds, in addition to the ice fraction of altostratus, altocumulus, nimbostratus, cumulus, stratocumulus, and stratus clouds) are added together to produce the total IWP. Cirrus cloud is defined by ISCCP to have a cloud top pressure higher than 440 hPa. However, in the tropics, liquid water may exist above 440 hPa. To take this fact into account, in the tropics (30°S to 30°N), 1/3 of the cloud water in cirrus, cirrostratus, and deep convective clouds is assumed to be liquid. Beyond this region, all cloud water in cirrus, cirrostratus, and deep convective clouds is assumed to be in the ice phase. This approach is different from that adopted by *Eliasson et al.* [2011] since ice clouds in the tropics are not partially classified into liquid clouds by their method. The IWP from ISCCP is shown to be smaller than the newer estimates from CloudSat [*Eliasson et al.*, 2011]. Generally, the IWP from the PCT cases compares well with observations in the NH, while the YCT cases all overpredict the IWP in the NH. In the SH, all cases compare well with the ISCCP IWP, except for Phi_PCT, which underpredicts IWP by nearly 20 g m^{-2} around 60°S. The fact that the IWP predicted in the Phi_PCT and Mey_PCT cases agree fairly well with satellite observations in the NH shows that the Phillips DCI parameterization is able to correctly predict ice water contents with an online calculation of the aerosol fields. The Mey_PCT simulation compares well with satellite observations of IWP in the SH, which implies that the underprediction of IWP in the Phi_PCT simulation in the SH is due to the small amount of DCI IN predicted by the Phillips DCI freezing parameterization. The IWP predicted in the Phi_YCT simulation compares well to ISCCP observation, because of the more contact ice nuclei predicted from the Young parameterization. The underprediction of IWP in the SH by Phi_PCT suggests the possibility that there are missing sources of ice nuclei in the SH. Although the YCT cases are in better agreement with the observed IWP in the SH, they overpredict IWP in the NH.

3.7. Global Mean Radiation Budget and Cloud Parameters

[40] The global mean radiation budget and cloud water paths are summarized in Table 3. Switching from the Meyers parameterization to the Phillips DCI freezing parameterization results in a net cloud forcing (NCF) change of 0.02 and -0.17 W m^{-2}, for the YCT and PCT cases, respectively. Switching from the YCT to the PCT contact freezing parameterization results in a NCF change of -4.99 and -5.18 W m^{-2}, for the Mey and Phi cases, respectively. *DeMott et al.* [2010] reported a global net cloud forcing change of -1.3 W m^{-2} associated with switching from the Meyers parameterization to the *DeMott et al.* [2010] parameterization. Our results indicate that the treatment of contact freezing in mixed phase clouds can be even more important in radiation balance of the climate system. The net solar flux at top of atmosphere (FSNT) changes by as much as 8.73 W m^{-2} due to the use of different heterogeneous ice nucleation parameterizations in mixed phase clouds in our experiments (see Table 3). The net longwave flux at top of atmosphere changes by a smaller amount, with the largest difference being 3.52 W m^{-2}. The reason the longwave flux change is smaller than the shortwave flux change is because

Table 3. Summary of the Global Mean Radiation Budget and Cloud Water Paths[a]

	Obs	Mey_YCT	Phi_YCT	Mey_PCT	Phi_PCT	Phi_PCT_PImix	PCT PD-PI	Phi_YCT_PImix	YCT PD-PI
SWCF (W m^{-2})	−47 to −54	−45.16 ± 0.14	−45.33 ± 0.17	−51.88 ± 0.22	−53.63 ± 0.12	−53.90 ± 0.19	0.27 ± 0.18	−46.54 ± 0.18	1.21 ± 0.31
LWCF (W m^{-2})	22–30	24.34 ± 0.06	24.53 ± 0.08	26.06 ± 0.10	27.65 ± 0.04	27.77 ± 0.05	−0.11 ± 0.05	24.91 ± 0.08	−0.38 ± 0.10
NCF (W m^{-2})		−20.82 ± 0.14	−20.80 ± 0.12	−25.81 ± 0.19	−25.98 ± 0.08	−26.13 ± 0.17	0.15 ± 0.17	−21.63 ± 0.18	0.83 ± 0.26
LWP (g m^{-2})	50–87	59.39 ± 0.26	60.04 ± 0.50	79.06 ± 0.33	88.22 ± 0.29	88.86 ± 0.42	−0.64 ± 0.31	63.47 ± 0.35	−3.43 ± 0.84
IWP (g m^{-2})	21.2	26.42 ± 0.10	26.05 ± 0.06	20.62 ± 0.07	18.32 ± 0.06	18.09 ± 0.06	0.23 ± 0.10	24.82 ± 0.16	1.23 ± 0.14
Nd (10^{10} m^{-2})	4	2.08 ± 0.01	2.12 ± 0.02	3.34 ± 0.02	3.27 ± 0.02	3.28 ± 0.01	−0.01 ± 0.02	2.23 ± 0.01	−0.11 ± 0.03
Ni (10^{10} m^{-2})		0.028 ± 0.008	0.03 ± 0.01	0.02 ± 0.003	0.03 ± 0.01	0.028 ± 0.004	0.0008 ± 0.002	0.025 ± 0.004	0.006 ± 0.005
IN_DCI (10^{10} m^{-2})		0.0022 ± 7e-6	0.0035 ± 1e-4	0.0023 ± 1e-5	0.0036 ± 1e-4	0.0033 ± 1e-4	0.0003 ± 2e-4	0.0032 ± 2e-4	0.0003 ± 2e-4
IN_CON (10^{10} m^{-2})		79.78 ± 2.17	78.15 ± 2.41	0.0085 ± 1e-4	0.0087 ± 3e-4	0.0068 ± 2e-4	0.0019 ± 4e-4	44.41 ± 1.14	33.74 ± 2.11
TCC (%)	0.65–0.67	0.682 ± 0.001	0.682 ± 0.001	0.688 ± 5e-4	0.689 ± 6e-4	0.689 ± 7e-4	−0.00005 ± 1e-3	0.683 ± 0.002	−0.001 ± 0.002
Ptot (mm d^{-1})	2.61	2.926 ± 0.004	2.93 ± 0.01	2.94 ± 0.01	2.93 ± 0.004	2.928 ± 0.004	0.0005 ± 0.001	2.93 ± 0.01	−0.001 ± 0.012
FSNT(W m^{-2})		243.78 ± 0.15	243.60 ± 0.13	236.71 ± 0.19	235.05 ± 0.12	234.77 ± 0.20	0.28 ± 0.19	242.43 ± 0.17	1.17 ± 0.25
FLNT(W m^{-2})		−238.47 ± 0.09	−238.24 ± 0.07	−236.228 ± 0.14	−234.95 ± 0.12	−234.83 ± 0.15	−0.12 ± 0.08	−237.99 ± 0.15	−0.24 ± 0.11

[a]Global mean shortwave cloud forcing (SWCF), longwave cloud forcing (LWCF), net cloud forcing (NCF), liquid water path (LWP), ice water path (IWP), vertically integrated cloud droplet number concentration (Nd) and ice crystal number concentration (Ni), vertically integrated DCI freezing ice nuclei (IN_DCI) and contact freezing ice nuclei (IN_CON) number concentration, total cloud cover (TCC), total precipitation (Ptot), net solar flux at top of atmosphere (FSNT), and net longwave radiation at top of atmosphere (FLNT) from the experiments described in Table 2. The shortwave (SWCF) and longwave (LWCF) cloud forcing observations are taken from ERBE for the years 1985–1989 [*Kiehl and Trenberth*, 1997] and CERES for the years 2000–2005 (http://ceres.larc.nasa.gov). In addition, the longwave (LWCF) cloud forcing from TOVS retrievals [*Susskind et al.*, 1997; *Scott et al.*, 1999] is included. The liquid water path (LWP) observations are from SSM/I (for the years 1987–1994, *Ferraro et al.* [1996]; for August 1993 and January 1994, *Weng and Grody* [1994]; and for August 1987 and February 1998, *Greenwald et al.* [1993]) and ISCCP for the year 1987 [*Han et al.*, 1994], and MODIS Terra data for 2001–2005 (http://modis.gsfc.nasa.gov/). The SSM/I data are restricted to the oceans. Ice water path (IWP) has been derived from ISCCP data for the years 1983–2000 (http://isccp.giss.nasa.gov/). Observation of Nd is obtained from ISCCP for the year 1987 [*Han et al.*, 1998]. Total cloud cover (TCC) is obtained from ISCCP D data for the years 1983–2001 [*Rossow and Schiffer*, 1999] and MODIS for the years 2001–2004 [*Platnick et al.*, 2003]. Total precipitation (Ptot) is taken from the Global Precipitation Data Set for the years 1979–2002 (http://precip.gsfc.nasa.gov).

of the height and temperature of mixed phase clouds. Unlike cirrus clouds, which are higher and thus much cooler compared to the surface, mixed phase clouds are lower, so do not have as large a longwave warming effect as cirrus clouds.

3.8. Anthropogenic Aerosol Effects in Mixed Phase Clouds

[41] Two additional simulations, Phi_PCT_PImix, and Phi_YCT_PImix were performed, in order to estimate the overall impact of mixed phase clouds on climate forcing. In these simulations, we carried separate PI BC/OM but we only allowed the PI concentrations to affect the heterogeneous freezing in mixed phase clouds, in order to gauge only changes in these clouds. So although BC/OM particles contribute to droplet formation in the model, the amount of droplet activation should be close to the same between PD and PImix runs. We estimate the anthropogenic aerosol effects in mixed phase clouds by taking the difference between the Phi_PCT and Phi_PCT_PImix simulations, and between the Phi_YCT and the Phi_YCT_PImix simulations. The differences in the global average radiation fluxes are summarized in Table 3. The increase in BC/OM concentrations from preindustrial to present-day in mixed phase clouds leads to increases of 9.1% and 27.9% in the DCI ice nuclei and contact ice nuclei, respectively, in the PCT simulations, and increases of 9.4% and 75% in the DCI ice nuclei and contact ice nuclei, respectively, in the YCT simulations. Ice crystal number concentrations increase by 7.14% between the Phi_PCT and Phi_PCT_PImix cases, and by 20% between the Phi_YCT and Phi_YCT_PImix cases. This also leads to a slight increase in IWP. At the same time, LWP and cloud droplet number are decreased because of the Bergeron-Findeisen process. This leads to smaller reflectivity of solar radiation, and larger transitivity of longwave radiation by mixed phase clouds in the PD scenario. Therefore, the SWCF and LWCF both decreased in absolute value from PI to PD. The net cloud forcing (NCF) change from preindustrial to present-day is 0.15 W m^{-2} in the PCT simulations, and 0.83 W m^{-2} in the YCT simulations. Both of these changes are statistically significant. So the anthropogenic aerosol effect in mixed phase clouds is a warming effect from our simulations. This NCF change is caused by changes in the number concentrations in mixed phase clouds as well as changes due to feedbacks, since both cloud albedo and lifetime effects are included as well as other feedbacks within the cloud systems.

[42] *Storelvmo et al.* [2011] also provided estimates of the effect of anthropogenic emissions of BC on mixed phase clouds (−0.32 to 0.23 W m^{-2}). Their preindustrial simulations are carried out with all aerosol emissions except BC the same as present-day simulations. They assume that the effects of BC on liquid clouds are negligible, because BC particles in their model are assumed to be largely hydrophobic. The NCF changes predicted from *Storelvmo et al.* [2011] with heterogeneous freezing parameterization of *Diehl et al.* [2006] and *Hoose et al.* [2010] are positive. The only negative NCF change (−0.32 W m^{-2}) is from the simulation where the *DeMott et al.* [2010] parameterization is used [*Storelvmo et al.*, 2011, Table 3]. They suggested that it is because the *DeMott et al.* [2010] parameterization is only based on large (>0.5 μm) particle concentration, which is mostly from natural sources. The concentration of these

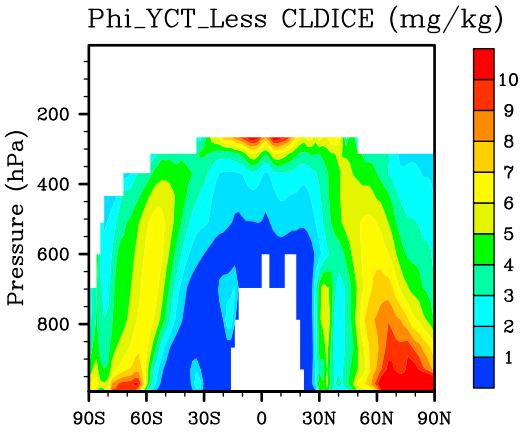

Figure 10. Zonal and annual mean latitude versus pressure plots of ice water mixing ratio in mixed phase clouds for sensitivity test Phi_YCT_Less.

natural particles decrease in PD because of more soluble coating, which leads to smaller ice nuclei concentration in PD. The 0.15 W m^{-2} forcing predicted by the PCT simulation lies within the range of forcings predicted by *Storelvmo et al.* [2011] (−0.32 to 0.23 W m^{-2}). The 0.83 W m^{-2} forcing predicted by the YCT simulation is beyond that range.

[43] The total shortwave forcing produced by heterogeneous freezing of anthropogenic BC in mixed phase clouds is calculated by taking the difference between the net solar flux at top of model (FSNT) between the Phi_PCT and Phi_PCT_PImix cases, and between the Phi_YCT and Phi_YCT_PImix cases. These are estimated to be 0.28 W m^{-2} for the PCT case, and 1.17 W m^{-2} for the YCT case. This total forcing includes the net cloud forcing, as well as the forcing due to feedbacks in meteorology fields such as water vapor. However, the effect of water vapor on the shortwave radiation is small. The total longwave forcing, which is calculated similarly, is smaller than the shortwave forcing for reasons explained in section 3.7. It is estimated to be −0.12 W m^{-2} for the PCT cases, and −0.24 W m^{-2} for the YCT cases. So the total climate forcing from anthropogenic BC/OM in mixed phase clouds is estimated to be 0.16–0.93 W m^{-2} using the aerosol-dependent parameterizations. These ranges of forcing changes reflects the uncertainty caused by different treatments of contact freezing in mixed phase clouds, the narrowing of which deserves further research effort.

[44] Here we caution that our comparison results are not meant to tell which of the parameterizations is the most realistic. Since these comparison results depend to a large extent on the fraction of BC/OM that is assumed to be contact IN. Due to the abundance of biomass burning and fossil fuel burning BC/OM particles, assuming only 1% versus 100% of BC/OM acting as contact IN would make a large difference. Here, we assumed that the hydrophobic fraction of fossil fuel BC/OM fraction that could act as contact IN was 17%. The smaller the hydrophobic fraction, the closer the Young parameterization will be to the Phillips contact freezing parameterization. Eventually, one can assume a hydrophobic fraction so that the two contact freezing parameterizations match each other. We confirm this supposition by adding a sensitivity test with a smaller percentage of dust and BC/OM acting as contact IN in the *Young* [1974] contact freezing parameterization in section 3.9. In a subsequent study, the number concentration of BC/OM that act as contact IN will be predicted based on online calculations of the hygroscopicity.

3.9. Sensitivity to the Contact Ice Nuclei Assumed in the Young Parameterization

[45] Here we examine a sensitivity simulation Phi_YCT_Less, where the fractions of dust and BC/OM that act as contact ice nuclei in the *Young* [1974] parameterization are greatly reduced. The original *Young* [1974] parameterization was derived from the experimental data of *Blanchard* [1957], which was conducted in winter in Massachusetts. The number concentration of contact ice nuclei was determined by *Young* [1974] to be 0.2 cm^{-3} at −4°C at sea level. Here, we match this value based on adjusting the concentration of BC/OM and dust particles at −4°C at sea level to obtain 0.2 cm^{-3} at the same season and location as the *Blanchard* [1957] measurements. We also assume that the fraction of dust that act as contact ice nuclei is 10 times larger than the fraction of BC/OM, to take into account that dust is a better ice nuclei. The factor of 10 is taken from the prediction of the *Phillips et al.* [2008] parameterization, where the frozen fraction of dust is about 10 times larger than soot from −3∼−40°C. The frozen fractions predicted by *Phillips et al.* [2008] parameterization have been shown to match well with observations [*Phillips et al.*, 2008]. Thus, instead of 100% of dust and 17% of BC/OM acting as contact ice nuclei, in Phi_YCT_Less, we use 0.2% of dust and 0.02% of BC/OM. The mixed phase cloud ice water mixing ratio for this sensitivity test is shown in Figure 10. Comparing Figure 10 to Figure 5, one sees that the mixed phase cloud ice water mixing ratio from this sensitivity test is very similar to the Phi_PCT case. The anthropogenic aerosol effect in mixed phase clouds calculated using this case is 0.71 W m^{-2}, which lies within the range of 0.16–0.93 W m^{-2} estimated using the Phi_PCT and Phi_YCT cases. The anthropogenic aerosol forcing is not very close to the Phi_PCT estimate, because the contribution of BC/OM to contact freezing in Phi_YCT_Less, similar to Phi_YCT, is still much larger than that from dust (figure not shown). In summary, if one assumes a smaller number concentration of, for example, hydrophobic BC/OM as contact ice nuclei, the ice concentrations in the YCT cases would decrease, becoming closer to the PCT cases, and there would be a smaller anthropogenic aerosol effect in mixed phase clouds.

4. Summary

[46] One parameterization for deposition/condensation/immersion ice nucleation and one for contact freezing in mixed phase clouds that depend on the aerosol size distribution and chemical composition are introduced into a coupled general circulation model and aerosol transport model. The present-day cloud liquid and ice water fields and the top of the atmosphere cloud radiative forcing are analyzed and compared to observations to see the effect of different heterogeneous freezing treatments.

[47] The DCI IN predicted using the Phillips parameterization shows a strong resemblance to the aerosol distribution.

Compared to the Meyers parameterization, The Phillips DCI freezing parameterization predicts more ice crystals in the middle troposphere and lower troposphere midlatitudes in the NH, and fewer ice crystals in the high-latitude NH and most of the SH. This leads to smaller IWP in the Phi DCI freezing cases especially in the SH. The smaller IWP in the SH from the Phi_PCT simulation leads to more cloud droplets and a larger LWP because of the less efficient Bergeron-Findeisen process. Therefore, the shortwave cloud forcing (SWCF) and longwave cloud forcing (LWCF) are larger in magnitude in the Phi_PCT simulation than in the Mey_PCT simulation in the SH. In the Mey_YCT and Phi_YCT cases, the effect of contact IN dominates in mixed phase clouds, which makes the changes predicted from using different DCI freezing parameterizations unimportant.

[48] The Phillips contact IN parameterization predicts 3 orders of magnitude less contact IN than the Young parameterization, and the contributions from dust and BC/OM are relatively equal. In the YCT cases, the contribution from BC/OM is much larger than that from dust. Deposition/condensation/immersion freezing dominates in the PCT cases, while contact freezing dominates in the YCT cases, unless the number of contact ice nuclei are reduced to the reference value on which the *Young* [1974] parameterization was based. Less cloud ice water and larger ice crystal effective radius are predicted in the PCT cases. The global average effective droplet radius, droplet number concentration and cloud liquid mixing ratios and LWPs increase because of the less efficient Bergeron-Findeisen process. Therefore, the SWCF and LWCF are larger in magnitude for the cases that use the Phillips contact freezing parameterization. The influences of using different contact freezing parameterizations on the cloud liquid and ice field are more pronounced than that from changing the DCI parameterization from Meyers to Phillips.

[49] When using the Phillips DCI freezing parameterization, the possibility for a given grid box to have low ice fraction is increased, while that for a given grid box to have a mixture of ice and liquid in decreased than when using Meyers parameterization. When using the Phillips contact freezing parameterization, the possibility for a given grid box to have low ice fraction is also increased compared to that using the Young parameterization. The above changes to the probability distribution of ice fractions further affect the cloud optical thickness observed at middle cloud altitudes.

[50] When using the Phillips DCI freezing parameterization and contact freezing parameterization, the optical thickness of middle clouds is increased. As a result, the cloud fractions of altostratus and nimbostratus clouds are increased, and that of altocumulus clouds are decreased compared to using the Meyers parameterization, or the Young parameterization. Therefore, the comparison of altostratus and nimbostratus clouds to ISCCP is improved, while the comparison of altocumulus clouds to ISCCP is worsened.

[51] In the SH, all cases except Phi_PCT are in reasonable agreement with observations of IWP. The IWP from the PCT cases compares well with observations in the NH, while the YCT cases over predict IWP in the NH. The fact that Phi_PCT and Mey_PCT agree fairly well with satellite observations in the NH shows that the Phillips DCI freezing parameterization is able to correctly predict ice water contents using an online calculation of aerosol fields. The underprediction of IWP in the SH by Phi_PCT, however, suggests the possibility that there are missing sources of ice nuclei in the SH.

[52] Switching from the Meyers parameterization to the Phillips DCI freezing parameterization results in an NCF change of 0.02 and -0.17 W m^{-2}, for the YCT and PCT cases, respectively. The net solar flux at top of atmosphere (FSNT), and net longwave flux at top of atmosphere (FLNT) also changes by up to 8.73 and 3.52 W m^{-2}, respectively, due to the use of different heterogeneous ice nucleation parameterizations in mixed phase clouds. This indicates that treatment of heterogeneous freezing in mixed phase clouds is important for the radiation balance of the climate system.

[53] The anthropogenic effects of BC/OM in mixed phase clouds are estimated. A net cloud forcing of 0.15 W m^{-2} is calculated for the PCT simulations and 0.83 W m^{-2} for the YCT simulations. The total shortwave climate forcing of anthropogenic BC/OM in mixed phase cloud is 0.28 W m^{-2} for the PCT cases, and 1.17 W m^{-2} for the YCT cases. The total longwave climate forcing of anthropogenic BC/OM in mixed phase cloud is estimated to be -0.12 W m^{-2} for the PCT cases, and -0.24 W m^{-2} for the YCT cases. So the total climate forcing from anthropogenic BC/OM in mixed phase clouds is 0.16–0.93 W m^{-2} using the aerosol-dependent freezing parameterizations. This range of forcing change reflects the uncertainty caused by different treatments of contact freezing in mixed phase clouds, the narrowing of which deserves further research effort.

[54] Our results are not intended to delineate which of the parameterizations is best, because of the uncertainties associated with the satellite data and comparison technique, as well as assumptions about which aerosol components act as contact freezing ice nuclei in the *Young* [1974] parameterization. When number concentration of dust and BC/OM contact ice nuclei is matched to the 0.2 cm^{-3} assumed in the original *Young* [1974] parameterization, the cloud ice mixing ratio is close to that in the Phi_PCT cases, and produces a smaller anthropogenic aerosol effect of 0.71 W m^{-2} in mixed phase clouds.

[55] **Acknowledgments.** We would like to thank Minghuai Wang at Pacific Northwest National Laboratory (PNNL) for his generosity in providing many helpful and constructive comments. We would also like to thank Xiaohong Liu at PNNL for his support and help. We are grateful to Alexei Korolev for providing observational data used in Figure 7. We also thank Karoline Diehl for discussions about contact freezing parameterizations and Trude Storelvmo for discussions regarding satellite observations of LWP and IWP. We greatly appreciate Roy (Yibin) Chen at University of Michigan for his help. We would also like to thank Xianglei Huang at University of Michigan for discussions about cloud radiative forcing. Three anonymous reviews and the Editor Steven Ghan provided many thoughtful and constructive comments that helped to improve this work. NSF project 35201095 funded this work. Computer time was provided by the NCAR CISL facility.

References

Abdul-Razzak, H., and S. J. Ghan (2000), A parameterization of aerosol activation: 2. Multiple aerosol types, *J. Geophys. Res.*, *105*(D5), 6837–6844, doi:10.1029/1999JD901161.

Abdul-Razzak, H., and S. J. Ghan (2002), A parameterization of aerosol activation: 3. Sectional representation, *J. Geophys. Res.*, *107*(D3), 4026, doi:10.1029/2001JD000483.

Archuleta, C. M., P. J. DeMott, and S. M. Kreidenweis (2005), Ice nucleation by surrogates for atmospheric mineral dust and mineral dust/sulfate particles at cirrus temperatures, *Atmos. Chem. Phys.*, *5*, 2617–2634, doi:10.5194/acp-5-2617-2005.

Barahona, D., J. Rodriguez, and A. Nenes (2010), Sensitivity of the global distribution of cirrus ice crystal concentration to heterogeneous freezing, *J. Geophys. Res.*, *115*, D23213, doi:10.1029/2010JD014273.

Berezinski, N. A., G. V. Stepanov, and V. G. Khorguani (1988), Ice-forming activity of atmospheric aerosol particles of different sizes, in *Atmospheric Aerosols and Nucleation*, *Lect. Notes Phys.*, vol. 309, pp. 709–712, Springer, Berlin.

Blanchard, D. C. (1957), The supercooling, freezing and melting of giant waterdrops at terminal velocity in air, in *Artificial Simulation of Rain*, edited by H. Weickmann, pp. 233–249, Pergamon, London.

Boville, B. A., P. J. Rasch, J. J. Hack, and J. R. McCaa (2006), Representation of clouds and precipitation processes in the Community Atmosphere Model version 3(CAM3), *J. Clim.*, *19*(11), 2184–2198, doi:10.1175/JCLI3749.1.

Chen, J. P., A. Hazra, and Z. Levin (2008), Parameterizing ice nucleation rates using contact angle and activation energy derived from laboratory data, *Atmos. Chem. Phys.*, *8*(24), 7431–7449.

Chen, Y. L., S. M. Kreidenweis, L. M. McInnes, D. C. Rogers, and P. J. DeMott (1998), Single particle analyses of ice nucleating aerosols in the upper troposphere and lower stratosphere, *Geophys. Res. Lett.*, *25*(9), 1391–1394, doi:10.1029/97GL03261.

Collins, W. D., P. J. Rasch, B. E. Eaton, B. V. Khattatov, J. F. Lamarque, and C. S. Zender (2001), Simulating aerosols using a chemical transport model with assimilation of satellite aerosol retrievals: Methodology for INDOEX, *J. Geophys. Res.*, *106*(D7), 7313–7336, doi:10.1029/2000JD900507.

Collins, W. D., P. J. Rasch, B. A. Boville, J. J. Hack, J. R. McCaa, D. L. Williamson, B. P. Briegleb, C. M. Bitz, S. J. Lin, and M. H. Zhang (2006a), The formulation and atmospheric simulation of the Community Atmosphere Model version 3(CAM3), *J. Clim.*, *19*(11), 2144–2161, doi:10.1175/JCLI3760.1.

Collins, W. D., et al. (2006b), The Community Climate System Model version 3(CCSM3), *J. Clim.*, *19*(11), 2122–2143, doi:10.1175/JCLI3761.1.

Connolly, P. J., O. Moehler, P. R. Field, H. Saathoff, R. Burgess, T. Choularton, and M. Gallagher (2009), Studies of heterogeneous freezing by three different desert dust samples, *Atmos. Chem. Phys.*, *9*, 2805–2824, doi:10.5194/acp-9-2805-2009.

Cooper, W. A. (1986), Ice initiation in natural clouds, in *Precipitation Enhancement—A Scientific Challenge*, *Meteorol. Monogr.*, vol. 21, edited by R. G. Braham Jr., pp. 29–32, Am. Meteorol. Soc., Boston, Mass.

Cziczo, D. J., D. M. Murphy, P. K. Hudson, and D. S. Thomson (2004), Single particle measurements of the chemical composition of cirrus ice residue during CRYSTAL-FACE, *J. Geophys. Res.*, *109*, D04201, doi:10.1029/2003JD004032.

DeMott, P. J. (1990), An exploratory-study of ice nucleation by soot aerosols, *J. Appl. Meteorol.*, *29*(10), 1072–1079, doi:10.1175/1520-0450(1990)029<1072:AESOIN>2.0.CO;2.

DeMott, P. J., D. J. Cziczo, A. J. Prenni, D. M. Murphy, S. M. Kreidenweis, D. S. Thomson, R. Borys, and D. C. Rogers (2003), Measurements of the concentration and composition of nuclei for cirrus formation, *Proc. Natl. Acad. Sci. U. S. A.*, *100*(25), 14,655–14,660, doi:10.1073/pnas.2532677100.

DeMott, P. J., A. J. Prenni, X. Liu, S. M. Kreidenweis, M. D. Petters, C. H. Twohy, M. S. Richardson, T. Eidhammer, and D. C. Rogers (2010), Predicting global atmospheric ice nuclei distributions and their impacts on climate, *Proc. Natl. Acad. Sci. U. S. A.*, *107*(25), 11,217–11,222, doi:10.1073/pnas.0910818107.

Diehl, K., and S. K. Mitra (1998), A laboratory study of the effects of a kerosene-burner exhaust on ice nucleation and the evaporation rate of ice crystals, *Atmos. Environ.*, *32*(18), 3145–3151, doi:10.1016/S1352-2310(97)00467-6.

Diehl, K., and S. Wurzler (2004), Heterogeneous drop freezing in the immersion mode: Model calculations considering soluble and insoluble particles in the drops, *J. Atmos. Sci.*, *61*(16), 2063–2072, doi:10.1175/1520-0469(2004)061<2063:HDFITI>2.0.CO;2.

Diehl, K., M. Simmel, and S. Wurzler (2006), Numerical sensitivity studies on the impact of aerosol properties and drop freezing modes on the glaciation, microphysics, and dynamics of clouds, *J. Geophys. Res.*, *111*, D07202, doi:10.1029/2005JD005884.

Eidhammer, T., P. J. DeMott, and S. M. Kreidenweis (2009), A comparison of heterogeneous ice nucleation parameterizations using a parcel model framework, *J. Geophys. Res.*, *114*, D06202, doi:10.1029/2008JD011095.

Eidhammer, T., et al. (2010), Ice initiation by aerosol particles: Measured and predicted ice nuclei concentrations versus measured ice crystal concentrations in an orographic wave cloud, *J. Atmos. Sci.*, *67*(8), 2417–2436, doi:10.1175/2010JAS3266.1.

Eliasson, S., S. A. Buehler, M. Milz, P. Eriksson, and V. O. John (2011), Assessing observed and modelled spatial distributions of ice water path using satellite data, *Atmos. Chem. Phys.*, *11*, 375–391, doi:10.5194/acp-11-375-2011.

Ferraro, R. R., F. Z. Weng, N. C. Grody, and A. Basist (1996), An eight-year (1987–1994) time series of rainfall, clouds, water vapor, snow cover, and sea ice derived from SSM/I measurements, *Bull. Am. Meteorol. Soc.*, *77*(5), 891–905, doi:10.1175/1520-0477(1996)077<0891:AEYTSO>2.0.CO;2.

Field, P. R., O. Mohler, P. Connolly, M. Kramer, R. Cotton, A. J. Heymsfield, H. Saathoff, and M. Schnaiter (2006), Some ice nucleation characteristics of Asian and Saharan desert dust, *Atmos. Chem. Phys.*, *6*, 2991–3006, doi:10.5194/acp-6-2991-2006.

Fletcher, N. H. (1962), *The Physics of Rain Clouds*, 386 pp., Cambridge Univ. Press, New York.

Friedman, B., G. Kulkarni, J. Beránek, A. Zelenyuk, J. A. Thornton, and D. J. Cziczo (2011), Ice nucleation and droplet formation by bare and coated soot particles, *J. Geophys. Res.*, *116*, D17203, doi:10.1029/2011JD015999.

Gary, B. L. (2006), Mesoscale temperature fluctuations in the stratosphere, *Atmos. Chem. Phys.*, *6*, 4577–4589, doi:10.5194/acp-6-4577-2006.

Gary, B. L. (2008), Mesoscale temperature fluctuations in the Southern Hemisphere stratosphere, *Atmos. Chem. Phys.*, *8*, 4677–4681, doi:10.5194/acp-8-4677-2008.

Georgii, H. W., and J. Kleinjung (1967), Relations between the chemical composition of atmospheric aerosol particles and the concentration of natural ice nuclei, *J. Rech. Atmos.*, *1*, 145–156.

Gettelman, A., X. Liu, S. J. Ghan, H. Morrison, S. Park, A. J. Conley, S. A. Klein, J. Boyle, D. L. Mitchell, and J.-L. F. Li (2010), Global simulations of ice nucleation and ice supersaturation with an improved cloud scheme in the Community Atmosphere Model, *J. Geophys. Res.*, *115*, D18216, doi:10.1029/2009JD013797.

Gorbunov, B., A. Baklanov, N. Kakutkina, H. L. Windsor, and R. Toumi (2001), Ice nucleation on soot particles, *J. Aerosol Sci.*, *32*(2), 199–215, doi:10.1016/S0021-8502(00)00077-X.

Greenwald, T. J., G. L. Stephens, T. H. Vonderhaar, and D. L. Jackson (1993), A physical retrieval of cloud liquid water over the global oceans using special sensor microwave imager (SSM/I) observations, *J. Geophys. Res.*, *98*(D10), 18,471–18,488, doi:10.1029/93JD00339.

Han, Q. Y., W. B. Rossow, and A. A. Lacis (1994), Near-global survey of effective droplet radii in liquid water clouds using ISCCP data, *J. Clim.*, *7*(4), 465–497, doi:10.1175/1520-0442(1994)007<0465:NGSOED>2.0.CO;2.

Han, Q. Y., W. B. Rossow, J. Chou, and R. M. Welch (1998), Global variation of column droplet concentration in low-level clouds, *Geophys. Res. Lett.*, *25*(9), 1419–1422, doi:10.1029/98GL01095.

Herzog, M., D. K. Weisenstein, and J. E. Penner (2004), A dynamic aerosol module for global chemical transport models: Model description, *J. Geophys. Res.*, *109*, D18202, doi:10.1029/2003JD004405.

Hobbs, P. V., G. C. Bluhm, and T. Ohtake (1971a), Transport of ice nuclei over North Pacific Ocean, *Tellus*, *23*(1), 28, doi:10.1111/j.2153-3490.1971.tb00544.x.

Hobbs, P. V., C. M. Fullerton, and G. C. Bluhm (1971b), Ice nucleus storms in Hawaii, *Nat. Phys. Sci.*, *230*(12), 90–91, doi:10.1038/physci230090a0.

Hoose, C., J. E. Kristjansson, J. P. Chen, and A. Hazra (2010), A classical-theory-based parameterization of heterogeneous ice nucleation by mineral dust, soot, and biological particles in a global climate model, *J. Atmos. Sci.*, *67*(8), 2483–2503, doi:10.1175/2010JAS3425.1.

Isono, K., and Y. Ibeke (1960), On the ice-nucleating ability of rockforming minerals and soil particles, *J. Meteorol. Soc. Jpn.*, *38*, 213–230.

Isono, K., M. Komabayasi, T. Takeda, and T. Tanaka (1970), *Concentration and nature of ice nuclei in the rim of the North Pacific Ocean, NWAP Rep. 70-R*, Water Resour. Lab., Nagoya Univ., Nagoya, Japan.

Kanji, Z. A., P. J. DeMott, O. Mohler, and J. P. D. Abbatt (2011), Results from the Univ. of Toronto continuous flow diffusion chamber at ICIS 2007: Instrument intercomparison and ice onsets for different aerosol types, *Atmos. Chem. Phys.*, *11*, 31–41, doi:10.5194/acp-11-31-2011.

Kärcher, B., and U. Lohmann (2003), A parameterization of cirrus cloud formation: Heterogeneous freezing, *J. Geophys. Res.*, *108*(D14), 4402, doi:10.1029/2002JD003220.

Khvorostyanov, V. I., and J. A. Curry (2004), The theory of ice nucleation by heterogeneous freezing of deliquescent mixed CCN. Part I: Critical radius, energy, and nucleation rate, *J. Atmos. Sci.*, *61*(22), 2676–2691, doi:10.1175/JAS3266.1.

Kiehl, J. T., and K. E. Trenberth (1997), Earth's annual global mean energy budget, *Bull. Am. Meteorol. Soc.*, *78*(2), 197–208, doi:10.1175/1520-0477(1997)078<0197:EAGMEB>2.0.CO;2.

Koehler, K. A., S. M. Kreidenweis, P. J. DeMott, A. J. Prenni, and M. D. Petters (2007), Potential impact of Owens (dry) Lake dust on warm and cold cloud formation, *J. Geophys. Res.*, *112*, D12210, doi:10.1029/2007JD008413.

Koehler, K. A., S. M. Kreidenweis, P. J. DeMott, M. D. Petters, A. J. Prenni, and O. Mohler (2010), Laboratory investigations of the impact of mineral dust aerosol on cold cloud formation, *Atmos. Chem. Phys.*, *10*, 11,955–11,968, doi:10.5194/acp-10-11955-2010.

Korolev, A. V., G. A. Isaac, S. G. Cober, J. W. Strapp, and J. Hallett (2003), Microphysical characterization of mixed-phase clouds, *Q. J. R. Meteorol. Soc.*, *129*(587), 39–65, doi:10.1256/qj.01.204.

Kulkarni, G., and S. Dobbie (2010), Ice nucleation properties of mineral dust particles: Determination of onset RH_i, IN active fraction, nucleation time-lag, and the effect of active sites on contact angles, *Atmos. Chem. Phys.*, *10*, 95–105, doi:10.5194/acp-10-95-2010.

Lee, S. S., and J. E. Penner (2010), Aerosol effects on ice clouds: Can the traditional concept of aerosol indirect effects be applied to aerosol-cloud interactions in cirrus clouds?, *Atmos. Chem. Phys.*, *10*, 10,345–10,358, doi:10.5194/acp-10-10345-2010.

Lin, W. Y., and M. H. Zhang (2004), Evaluation of clouds and their radiative effects simulated by the NCAR Community Atmospheric Model against satellite observations, *J. Clim.*, *17*(17), 3302–3318, doi:10.1175/1520-0442(2004)017<3302:EOCATR>2.0.CO;2.

Liu, X., and J. E. Penner (2002), Effect of Mount Pinatubo H_2SO_4/H_2O aerosol on ice nucleation in the upper troposphere using a global chemistry and transport model, *J. Geophys. Res.*, *107*(D12), 4141, doi:10.1029/2001JD000455.

Liu, X., and J. E. Penner (2005), Ice nucleation parameterization for global models, *Meteorol. Z.*, *14*(4), 499–514, doi:10.1127/0941-2948/2005/0059.

Liu, X., J. E. Penner, and M. Herzog (2005), Global modeling of aerosol dynamics: Model description, evaluation, and interactions between sulfate and nonsulfate aerosols, *J. Geophys. Res.*, *110*, D18206, doi:10.1029/2004JD005674.

Liu, X., J. E. Penner, S. J. Ghan, and M. Wang (2007), Inclusion of ice microphysics in the NCAR community atmospheric model version 3 (CAM3), *J. Clim.*, *20*(18), 4526–4547, doi:10.1175/JCLI4264.1.

Lohmann, U. (2002), Possible aerosol effects on ice clouds via contact nucleation, *J. Atmos. Sci.*, *59*(3), 647–656, doi:10.1175/1520-0469(2001)059<0647:PAEOIC>2.0.CO;2.

Lohmann, U., and K. Diehl (2006), Sensitivity studies of the importance of dust ice nuclei for the indirect aerosol effect on stratiform mixed-phase clouds, *J. Atmos. Sci.*, *63*(3), 968–982, doi:10.1175/JAS3662.1.

Lohmann, U., and C. Hoose (2009), Sensitivity studies of different aerosol indirect effects in mixed-phase clouds, *Atmos. Chem. Phys.*, *9*, 8917–8934, doi:10.5194/acp-9-8917-2009.

Lohmann, U., P. Stier, C. Hoose, S. Ferrachat, S. Kloster, E. Roeckner, and J. Zhang (2007), Cloud microphysics and aerosol indirect effects in the global climate model ECHAM5-HAM, *Atmos. Chem. Phys.*, *7*, 3425–3446, doi:10.5194/acp-7-3425-2007.

Marcolli, C., S. Gedamke, T. Peter, and B. Zobrist (2007), Efficiency of immersion mode ice nucleation on surrogates of mineral dust, *Atmos. Chem. Phys.*, *7*, 5081–5091, doi:10.5194/acp-7-5081-2007.

Meyers, M. P., P. J. DeMott, and W. R. Cotton (1992), New primary ice-nucleation parameterizations in an explicit cloud model, *J. Appl. Meteorol.*, *31*(7), 708–721, doi:10.1175/1520-0450(1992)031<0708:NPINPI>2.0.CO;2.

Minikin, A., A. Petzold, J. Ström, R. Krejci, M. Seifert, P. van Velthoven, H. Schlager, and U. Schumann (2003), Aircraft observations of the upper tropospheric fine particle aerosol in the Northern and Southern Hemispheres at midlatitudes, *Geophys. Res. Lett.*, *30*(10), 1503, doi:10.1029/2002GL016458.

Monahan, E. C., and I. G. O'Muircheartaigh (1986), Whitecaps and the passive remote-sensing of the ocean surface, *Int. J. Remote Sens.*, *7*(5), 627–642, doi:10.1080/01431168608954716.

Muhlbauer, A., T. Hashino, L. Xue, A. Teller, U. Lohmann, R. M. Rasmussen, I. Geresdi, and Z. Pan (2010), Intercomparison of aerosol-cloud-precipitation interactions in stratiform orographic mixed-phase clouds, *Atmos. Chem. Phys.*, *10*, 8173–8196, doi:10.5194/acp-10-8173-2010.

Murray, B. J., S. L. Broadley, T. W. Wilson, J. D. Atkinson, and R. H. Wills (2011), Heterogeneous freezing of water droplets containing kaolinite particles, *Atmos. Chem. Phys.*, *11*, 4191–4207, doi:10.5194/acp-11-4191-2011.

Penner, J. E., D. J. Bergmann, J. J. Walton, D. Kinnison, M. J. Prather, D. Rotman, C. Price, K. E. Pickering, and S. L. Baughcum (1998), An evaluation of upper troposphere NOx with two models, *J. Geophys. Res.*, *103*(D17), 22,097–22,113, doi:10.1029/98JD01565.

Penner, J. E., et al. (2001), Aerosols, their direct and indirect effects, in *Report to IPCC From the Scientific Assessment Working Group (WGI)*, pp. 289–348, Cambridge Univ. Press, Cambridge, U. K.

Penner, J. E., Y. Chen, M. Wang, and X. Liu (2009), Possible influence of anthropogenic aerosols on cirrus clouds and anthropogenic forcing, *Atmos. Chem. Phys.*, *9*, 879–896, doi:10.5194/acp-9-879-2009.

Phillips, V. T. J., P. J. DeMott, and C. Andronache (2008), An empirical parameterization of heterogeneous ice nucleation for multiple chemical species of aerosol, *J. Atmos. Sci.*, *65*(9), 2757–2783, doi:10.1175/2007JAS2546.1.

Platnick, S., M. D. King, S. A. Ackerman, W. P. Menzel, B. A. Baum, J. C. Riedi, and R. A. Frey (2003), The MODIS cloud products: Algorithms and examples from Terra, *IEEE Trans. Geosci. Remote Sens.*, *41*(2), 459–473, doi:10.1109/TGRS.2002.808301.

Prenni, A. J., P. J. DeMott, C. Twohy, M. R. Poellot, S. M. Kreidenweis, D. C. Rogers, S. D. Brooks, M. S. Richardson, and A. J. Heymsfield (2007), Examinations of ice formation processes in Florida cumuli using ice nuclei measurements of anvil ice crystal particle residues, *J. Geophys. Res.*, *112*, D10221, doi:10.1029/2006JD007549.

Pruppacher, H. R., and J. D. Klett (1997), *Microphysics of Clouds and Precipitation*, 2nd ed., Kluwer Academic, Dordrecht, Netherlands.

Rasch, P. J., W. D. Collins, and B. E. Eaton (2001), Understanding the Indian Ocean Experiment (INDOEX) aerosol distributions with an aerosol assimilation, *J. Geophys. Res.*, *106*(D7), 7337–7355, doi:10.1029/2000JD900508.

Reddy, M. S., and O. Boucher (2004), A study of the global cycle of carbonaceous aerosols in the LMDZT general circulation model, *J. Geophys. Res.*, *109*, D14202, doi:10.1029/2003JD004048.

Richardson, M. S., et al. (2007), Measurements of heterogeneous ice nuclei in the western United States in springtime and their relation to aerosol characteristics, *J. Geophys. Res.*, *112*, D02209, doi:10.1029/2006JD007500.

Rossow, W. B., and R. A. Schiffer (1999), Advances in understanding clouds from ISCCP, *Bull. Am. Meteorol. Soc.*, *80*(11), 2261–2287, doi:10.1175/1520-0477(1999)080<2261:AIUCFI>2.0.CO;2.

Rotman, D. A., et al. (2004), IMPACT, the LLNL 3-D global atmospheric chemical transport model for the combined troposphere and stratosphere: Model description and analysis of ozone and other trace gases, *J. Geophys. Res.*, *109*, D04303, doi:10.1029/2002JD003155.

Rotstayn, L. D., B. F. Ryan, and J. J. Katzfey (2000), A scheme for calculation of the liquid fraction in mixed-phase stratiform clouds in large-scale models, *Mon. Weather Rev.*, *128*(4), 1070–1088, doi:10.1175/1520-0493(2000)128<1070:ASFCOT>2.0.CO;2.

Salzmann, M., Y. Ming, J. C. Golaz, P. A. Ginoux, H. Morrison, A. Gettelman, M. Kramer, and L. J. Donner (2010), Two-moment bulk stratiform cloud microphysics in the GFDL AM3 GCM: Description, evaluation, and sensitivity tests, *Atmos. Chem. Phys.*, *10*, 8037–8064, doi:10.5194/acp-10-8037-2010.

Santachiara, G., L. Di Matteo, F. Prodi, and F. Belosi (2010), Atmospheric particles acting as ice forming nuclei in different size ranges, *Atmos. Res.*, *96*(2–3), 266–272, doi:10.1016/j.atmosres.2009.08.004.

Schaefer, V. J. (1949), The formation of ice crystals in the laboratory and the atmosphere, *Chem. Rev.*, *44*, 291–320, doi:10.1021/cr60138a004.

Scott, N. A., A. Chedin, R. Armante, J. Francis, C. Stubenrauch, J. P. Chaboureau, F. Chevallier, C. Claud, and F. Cheruy (1999), Characteristics of the TOVS pathfinder Path-B dataset, *Bull. Am. Meteorol. Soc.*, *80*(12), 2679–2701, doi:10.1175/1520-0477(1999)080<2679:COTTPP>2.0.CO;2.

Seifert, A., C. Köhler, and K. D. Beheng (2011), Aerosol-cloud-precipitation effects over Germany as simulated by a convective-scale numerical weather prediction model, *Atmos. Chem. Phys. Discuss.*, *11*, 20,203–20,243, doi:10.5194/acpd-11-20203-2011.

Shaw, R. A., A. J. Durant, and Y. Mi (2005), Heterogeneous surface crystallization observed in undercooled water, *J. Phys. Chem. B*, *109*(20), 9865–9868, doi:10.1021/jp0506336.

Storelvmo, T., J. E. Kristjansson, and U. Lohmann (2008), Aerosol influence on mixed-phase clouds in CAM-Oslo, *J. Atmos. Sci.*, *65*(10), 3214–3230, doi:10.1175/2008JAS2430.1.

Storelvmo, T., C. Hoose, and P. Eriksson (2011), Global modeling of mixed-phase clouds: The albedo and lifetime effects of aerosols, *J. Geophys. Res.*, *116*, D05207, doi:10.1029/2010JD014724.

Susskind, J., P. Piraino, L. Rokke, T. Iredell, and A. Mehta (1997), Characteristics of the TOVS Pathfinder Path A dataset, *Bull. Am. Meteorol. Soc.*, *78*(7), 1449–1472, doi:10.1175/1520-0477(1997)078<1449:COTTPP>2.0.CO;2.

Targino, A. C., R. Krejci, K. J. Noone, and P. Glantz (2006), Single particle analysis of ice crystal residuals observed in orographic wave clouds over Scandinavia during INTACC experiment, *Atmos. Chem. Phys.*, *6*, 1977–1990, doi:10.5194/acp-6-1977-2006.

Vali, G. (1985), Nucleation terminology, *Bull. Am. Meteorol. Soc.*, *66*(11), 1426–1427.

Wang, L., Y. Q. Wang, A. Lauer, and S. P. Xie (2011), Simulation of seasonal variation of marine boundary layer clouds over the eastern Pacific with a regional climate model, *J. Clim.*, *24*(13), 3190–3210, doi:10.1175/2010JCLI3935.1.

Wang, M., and J. E. Penner (2010), Cirrus clouds in a global climate model with a statistical cirrus cloud scheme, *Atmos. Chem. Phys.*, *10*, 5449–5474, doi:10.5194/acp-10-5449-2010.

Wang, M., J. E. Penner, and X. Liu (2009), Coupled IMPACT aerosol and NCAR CAM3 model: Evaluation of predicted aerosol number and size distribution, *J. Geophys. Res.*, *114*, D06302, doi:10.1029/2008JD010459.

Warren, S. G., C. J. Hahn, J. London, R. M. Chervin, and R. L. Jenne (1986), Global distribution of total cloud cover and cloud type amounts over land, *NCAR Tech. Note, NCAR/TN-273+STR*, 29 pp. + 200 maps, Natl. Cent. for Atmos. Res., Boulder, Colo.

Warren, S. G., C. J. Hahn, J. London, R. M. Chervin, and R. L. Jenne (1988), Global distribution of total cloud cover and cloud type amounts over the ocean, *NCAR Tech. Note, NCAR/TN-317+STR*, 41 pp. + 170 maps, Natl. Cent. for Atmos. Res., Boulder, Colo.

Weng, F. Z., and N. C. Grody (1994), Retrieval of cloud liquid water using the special sensor microwave imager (SSM/I), *J. Geophys. Res.*, *99*(D12), 25,535–25,551, doi:10.1029/94JD02304.

Xie, S., J. Boyle, S. A. Klein, X. Liu, and S. Ghan (2008), Simulations of Arctic mixed-phase clouds in forecasts with CAM3 and AM2 for M-PACE, *J. Geophys. Res.*, *113*, D04211, doi:10.1029/2007JD009225.

Young, K. C. (1974), Numerical-simulation of wintertime, orographic precipitation. 1. Description of model microphysics and numerical techniques, *J. Atmos. Sci.*, *31*(7), 1735–1748, doi:10.1175/1520-0469(1974)031<1735:ANSOWO>2.0.CO;2.

Zhang, M., W. Lin, C. S. Bretherton, J. J. Hack, and P. J. Rasch (2003), A modified formulation of fractional stratiform condensation rate in the NCAR Community Atmospheric Model (CAM2), *J. Geophys. Res.*, *108*(D1), 4035, doi:10.1029/2002JD002523.

J. E. Penner and Y. Yun, Department of Atmospheric, Oceanic, and Space Sciences, University of Michigan, 2455 Hayward St., Ann Arbor, MI 48105, USA. (yuxingy@umich.edu)